Table 2. Combinations of Soluble Factors Determined by Fractional Factorial Design F, FGF-2; I, IGF-I; In, insulin; B, BMP-2; P, PTH; G, GH; D, Dex; V, vitD; T, T3; IL, IL-1 RA; E, E_2; Te, testosterone.

	F	I	in	B	P	G	D	V	T	IL	E	Te
1	+	+	+	+	+	+	+	+	+	+	+	+
2	+	+	+	+	+	+	+	−	−	−	−	−
3	+	+	+	+	+	+	−	+	−	+	+	−
4	+	+	+	+	+	+	−	+	−	+	−	+
5	+	+	+	+	+	+	−	−	−	−	+	+
6	+	+	+	+	+	−	+	+	−	−	−	+
7	+	+	+	+	+	−	+	−	+	−	+	−
8	+	+	+	+	+	−	−	−	+	+	−	+
9	+	+	+	+	−	+	+	+	+	−	−	−
10	+	+	+	+	−	+	+	+	−	+	+	+
11	+	+	+	+	−	+	−	+	+	+	+	−
12	+	+	+	+	−	+	−	−	+	+	−	−
13	+	+	+	+	−	+	−	−	−	−	+	−
14	+	+	+	+	−	−	+	+	+	+	−	−
15	+	+	+	+	−	−	+	+	+	−	+	+
16	+	+	+	+	−	−	+	−	−	+	+	+
17	+	+	+	+	−	−	+	−	−	−	−	+
18	+	+	+	−	+	+	+	+	+	+	+	−
19	+	+	+	−	+	+	+	+	+	−	−	−
20	+	+	+	−	+	+	−	+	−	−	+	+
21	+	+	+	−	+	+	−	−	+	+	+	+
22	+	+	+	−	+	−	+	+	−	+	+	+
23	+	+	+	−	+	−	−	+	+	−	+	−
24	+	+	+	−	+	−	−	+	−	−	−	−
25	+	+	+	−	+	−	−	−	+	−	+	−
26	+	+	+	−	+	−	−	−	−	+	−	+
27	+	+	+	−	−	+	+	−	+	+	+	−
28	+	+	+	−	−	+	+	−	+	−	−	+
29	+	+	+	−	−	+	+	−	−	+	−	+
30	+	+	+	−	−	+	−	+	+	−	−	+
31	+	+	+	−	−	−	+	+	−	−	+	−
32	+	+	+	−	−	−	+	−	−	+	−	−
33	+	+	+	−	−	−	−	+	+	−	−	+
34	+	+	+	−	−	−	−	−	−	+	+	+
35	+	+	−	+	+	+	+	+	+	+	−	−
36	+	+	−	+	+	+	+	+	+	−	+	+
37	+	+	−	+	+	+	+	−	−	+	+	−
38	+	+	−	+	+	+	−	+	+	−	−	−
39	+	+	−	+	+	+	−	−	+	−	−	−
40	+	+	−	+	+	−	+	+	−	+	−	−
41	+	+	−	+	+	−	−	−	+	−	+	+
42	+	+	−	+	+	−	−	−	−	+	+	−
43	+	+	−	+	−	+	+	−	+	−	+	−
44	+	+	−	+	−	+	+	−	−	+	−	+
45	+	+	−	+	−	+	−	+	−	−	−	+
46	+	+	−	+	−	−	+	−	−	−	−	−
47	+	+	−	+	−	−	−	+	+	+	−	+
48	+	+	−	+	−	−	−	+	−	−	+	+
49	+	+	−	−	+	+	+	+	−	+	−	−
50	+	+	−	−	+	+	−	−	+	+	−	+
51	+	+	−	−	+	+	−	−	−	−	+	+
52	+	+	−	−	+	−	+	+	+	+	+	+
53	+	+	−	−	+	−	+	−	−	+	+	−
54	+	+	−	−	+	−	+	−	−	−	−	+
55	+	+	−	−	+	−	−	+	+	+	−	−
56	+	+	−	−	+	−	−	−	+	−	−	+
57	+	+	−	−	−	+	+	+	+	+	+	+
58	+	+	−	−	−	+	+	+	−	−	+	−
59	+	+	−	−	−	+	−	−	+	−	+	+
60	+	+	−	−	−	+	−	−	−	+	−	−
61	+	+	−	−	−	−	+	−	+	+	−	+
62	+	+	−	−	−	−	+	−	+	−	−	−
63	+	+	−	−	−	−	−	+	+	+	+	−
64	+	+	−	−	−	−	−	+	−	−	−	−
65	+	−	+	+	+	+	+	+	+	+	+	−
66	+	−	+	+	+	+	+	−	+	−	−	+
67	+	−	+	+	+	+	+	−	−	+	−	−
68	+	−	+	+	+	+	−	+	+	−	+	+
69	+	−	+	+	+	−	+	−	−	−	+	+
70	+	−	+	+	+	−	−	+	+	+	+	+
71	+	−	+	+	+	−	−	+	−	+	−	−
72	+	−	+	+	+	−	−	+	−	−	+	−
73	+	−	+	+	−	+	+	+	−	−	−	+
74	+	−	+	+	−	+	+	−	+	+	+	+
75	+	−	+	+	−	+	−	+	−	+	−	−
76	+	−	+	+	−	+	−	−	+	−	+	−
77	+	−	+	+	−	−	+	+	−	+	+	−
78	+	−	+	+	−	−	−	−	+	−	−	+
79	+	−	+	+	−	−	−	−	+	−	−	−
80	+	−	+	+	−	−	−	−	−	+	−	+
81	+	−	+	−	+	+	+	+	+	+	−	+
82	+	−	+	−	+	+	+	−	−	−	+	+
83	+	−	+	−	+	+	−	−	+	+	−	−
84	+	−	+	−	+	+	−	−	−	+	+	−
85	+	−	+	−	+	+	−	−	−	−	−	−
86	+	−	+	−	+	−	+	−	+	+	+	+
87	+	−	+	−	+	−	+	−	+	−	−	−
88	+	−	+	−	+	−	−	+	+	−	−	+
89	+	−	+	−	−	+	+	+	−	−	+	−
90	+	−	+	−	−	+	−	+	+	+	+	+
91	+	−	+	−	−	−	+	+	+	+	−	+
92	+	−	+	−	−	−	+	+	+	+	−	−
93	+	−	+	−	−	−	−	+	−	−	+	+
94	+	−	+	−	−	−	−	−	+	+	+	−
95	+	−	+	−	−	−	−	−	−	−	+	−
96	+	−	−	+	+	+	+	+	−	−	+	+
97	+	−	−	+	+	+	+	−	+	+	−	−
98	+	−	−	+	+	+	−	+	+	+	−	+
99	+	−	−	+	+	+	−	+	−	−	+	−
100	+	−	−	+	+	+	−	−	−	+	+	+
101	+	−	−	+	+	−	+	+	+	−	−	−
102	+	−	−	+	+	−	+	+	−	+	−	+
103	+	−	−	+	+	−	−	−	+	+	+	−
104	+	−	−	+	+	−	−	−	−	−	−	+
105	+	−	−	+	−	+	+	+	+	+	+	−
106	+	−	−	+	−	+	+	+	−	+	−	−
107	+	−	−	+	−	+	−	−	+	+	−	+
108	+	−	−	+	−	+	−	−	−	+	+	+
109	+	−	−	+	−	−	+	+	+	−	−	+
110	+	−	−	+	−	−	+	−	+	+	+	−
111	+	−	−	+	−	−	+	−	−	−	+	+
112	+	−	−	+	−	−	−	+	+	−	+	−
113	+	−	−	+	−	−	−	+	−	−	−	−
114	+	−	−	−	+	+	+	−	+	−	+	−
115	+	−	−	−	+	+	−	+	+	+	+	−
116	+	−	−	−	+	+	−	+	−	−	−	+
117	+	−	−	−	+	−	+	+	−	−	+	−
118	+	−	−	−	+	−	+	−	+	+	−	−
119	+	−	−	−	+	−	−	+	+	−	+	+
120	+	−	−	−	+	−	−	−	−	−	−	−
121	+	−	−	−	−	+	+	+	+	−	−	−
122	+	−	−	−	−	+	+	−	−	−	−	+
123	+	−	−	−	−	+	−	+	+	−	−	−
124	+	−	−	−	−	+	−	+	−	+	+	−
125	+	−	−	−	−	−	+	+	−	+	+	+
126	+	−	−	−	−	−	+	−	+	−	+	+
127	+	−	−	−	−	−	+	−	−	+	−	−
128	+	−	−	−	−	−	−	+	−	+	−	+
129	−	+	+	+	+	+	+	+	−	+	−	+
130	−	+	+	+	+	+	+	+	−	−	−	−
131	−	+	+	+	+	+	−	−	+	−	−	+
132	−	+	+	+	+	−	+	+	+	+	+	+
133	−	+	+	+	+	−	+	−	+	+	−	−
134	−	+	+	+	+	−	+	−	−	+	−	−
135	−	+	+	+	+	−	−	+	+	−	−	+
136	−	+	+	+	+	−	−	−	−	−	+	+
137	−	+	+	+	−	+	+	−	−	+	+	+
138	−	+	+	+	−	+	−	+	+	−	+	+
139	−	+	+	+	−	+	−	−	+	+	−	−
140	−	+	+	+	−	+	−	−	−	−	−	+
141	−	+	+	+	−	−	+	+	+	−	+	−
142	−	+	+	+	−	−	+	−	+	−	−	−
143	−	+	+	+	−	−	−	+	−	+	+	−
144	−	+	+	+	−	−	−	+	−	−	−	−
145	−	+	+	−	+	+	+	+	−	−	+	+
146	−	+	+	−	+	+	+	−	+	−	−	+
147	−	+	+	−	+	+	−	+	+	−	+	−
148	−	+	+	−	+	+	−	−	−	+	+	−
149	−	+	+	−	+	−	+	+	−	+	+	−
150	−	+	+	−	+	−	+	−	−	+	−	+
151	−	+	+	−	+	−	−	+	+	+	−	+
152	−	+	+	−	−	+	+	+	+	+	−	−
153	−	+	+	−	−	+	+	−	−	−	+	−
154	−	+	+	−	−	+	−	+	−	+	−	+
155	−	+	+	−	−	+	−	+	−	+	−	−
156	−	+	+	−	−	−	+	+	+	+	+	+
157	−	+	+	−	−	−	+	−	+	−	+	+
158	−	+	+	−	−	−	−	+	+	+	+	−
159	−	+	+	−	−	−	−	−	+	+	+	+
160	−	+	+	−	−	−	−	−	−	−	−	−
161	−	+	−	+	+	+	+	−	−	−	+	+
162	−	+	−	+	+	+	−	+	+	+	+	−
163	−	+	−	+	+	+	−	+	−	−	−	−
164	−	+	−	+	+	−	+	+	+	−	+	−
165	−	+	−	+	+	−	+	−	+	+	+	+
166	−	+	−	+	+	−	−	+	−	+	+	+
167	−	+	−	+	+	−	−	+	−	+	−	−
168	−	+	−	+	−	+	+	+	+	+	−	−
169	−	+	−	+	−	+	+	+	−	−	+	−
170	−	+	−	+	−	+	+	−	+	−	−	+
171	−	+	−	+	−	+	−	−	+	+	+	+
172	−	+	−	+	−	+	−	−	−	+	+	−
173	−	+	−	+	−	−	+	+	−	+	+	−
174	−	+	−	+	−	−	−	+	+	−	−	+
175	−	+	−	+	−	−	−	−	+	−	+	−
176	−	+	−	+	−	−	−	−	−	+	−	+
177	−	+	−	−	+	+	+	−	+	+	+	−
178	−	+	−	−	+	+	+	−	−	−	−	−
179	−	+	−	−	+	+	−	+	+	+	+	+
180	−	+	−	−	+	+	−	−	−	+	−	+
181	−	+	−	−	+	−	+	+	+	−	−	+
182	−	+	−	−	+	−	+	+	+	−	−	−
183	−	+	−	−	+	−	−	+	−	−	+	+
184	−	+	−	−	+	−	−	−	+	+	−	−
185	−	+	−	−	+	−	−	−	−	−	+	−
186	−	+	−	−	−	+	+	+	−	−	−	+
187	−	+	−	−	−	+	−	+	+	−	+	−
188	−	+	−	−	−	+	−	+	−	+	+	+
189	−	+	−	−	−	+	−	−	+	−	−	−
190	−	+	−	−	−	−	+	+	−	+	−	+
191	−	+	−	−	−	−	+	−	+	+	+	−
192	−	+	−	−	−	−	+	−	−	−	+	+
193	−	−	+	+	+	+	+	+	+	+	−	+
194	−	−	+	+	+	+	+	+	+	−	−	−
195	−	−	+	+	+	+	+	+	−	−	+	−
196	−	−	+	+	+	+	−	−	+	+	+	−
197	−	−	+	+	+	+	−	−	−	+	−	+
198	−	−	+	+	+	−	+	+	−	−	+	+
199	−	−	+	+	+	−	−	+	+	+	−	−
200	−	−	+	+	+	−	−	+	−	−	−	+
201	−	−	+	+	+	−	−	−	−	−	+	−
202	−	−	+	+	−	+	+	+	+	−	+	+
203	−	−	+	+	−	+	+	−	+	−	+	−
204	−	−	+	+	−	+	−	+	+	−	−	−
205	−	−	+	+	−	+	−	+	−	+	+	+
206	−	−	+	+	−	−	+	+	−	+	−	+
207	−	−	+	+	−	−	+	−	+	+	−	+
208	−	−	+	+	−	−	+	−	−	+	+	−
209	−	−	+	+	−	−	−	−	+	+	+	+
210	−	−	+	−	+	+	+	+	−	+	+	+
211	−	−	+	−	+	+	−	+	+	−	−	−
212	−	−	+	−	+	+	−	−	+	−	+	+
213	−	−	+	−	+	−	+	+	+	+	+	−
214	−	−	+	−	+	−	+	−	+	−	+	+
215	−	−	+	−	+	−	+	−	−	−	−	−
216	−	−	+	−	+	−	−	+	−	+	−	−
217	−	−	+	−	+	−	−	−	−	+	+	+
218	−	−	+	−	−	+	+	−	+	+	+	−
219	−	−	+	−	−	+	+	−	−	+	−	−
220	−	−	+	−	−	+	−	+	−	−	+	−
221	−	−	+	−	−	+	−	+	+	+	−	+
222	−	−	+	−	−	+	−	−	−	−	−	+
223	−	−	+	−	−	−	+	+	−	−	−	+
224	−	−	+	−	−	−	+	−	+	−	−	−
225	−	−	+	−	−	−	−	+	+	−	+	−
226	−	−	−	+	+	+	+	+	−	+	+	+
227	−	−	−	+	+	+	−	−	+	−	+	+
228	−	−	−	+	+	+	−	−	−	+	−	−
229	−	−	−	+	+	−	+	+	+	+	−	−
230	−	−	−	+	+	−	+	−	+	−	−	+
231	−	−	−	+	+	−	+	−	−	−	+	−
232	−	−	−	+	+	−	−	−	+	−	−	−
233	−	−	−	+	−	+	+	−	−	−	−	−
234	−	−	−	+	−	+	−	+	+	+	+	−
235	−	−	−	+	−	+	−	+	+	+	−	+
236	−	−	−	+	−	+	−	−	−	−	+	+
237	−	−	−	+	−	−	+	+	+	+	+	+
238	−	−	−	+	−	−	−	+	−	−	+	+
239	−	−	−	+	−	−	−	−	−	+	−	−
240	−	−	−	−	+	+	+	+	+	−	−	+
241	−	−	−	−	+	+	+	+	−	+	−	−
242	−	−	−	−	+	+	+	−	+	+	−	+
243	−	−	−	−	+	+	+	−	+	−	+	−
244	−	−	−	−	+	+	−	+	−	−	−	+
245	−	−	−	−	+	−	+	−	−	+	−	+
246	−	−	−	−	+	−	−	+	−	+	+	−
247	−	−	−	−	+	−	−	−	+	+	+	+
248	−	−	−	−	−	+	+	+	+	−	+	+
249	−	−	−	−	−	+	+	−	−	+	+	+
250	−	−	−	−	−	+	−	−	+	+	−	−
251	−	−	−	−	−	+	−	−	−	−	+	−
252	−	−	−	−	−	−	+	+	+	−	+	−
253	−	−	−	−	−	−	+	+	−	−	−	−
254	−	−	−	−	−	−	−	+	+	+	−	+
255	−	−	−	−	−	−	−	−	+	−	−	+
256	−	−	−	−	−	−	−	−	−	+	+	−

RNA with the Superscript II reverse transcriptase kit (Invitrogen, Carlsbad, CA, USA). For the real-time PCR, the ABI Prism Sequence Detection System 7000 was used. Primers were designed based on the sequences obtained from the GenBank, and amplicons of 50–250 base pairs with a melting temperature of between 55°C and 60°C were selected. Aliquots of the first-strand cDNA (1 μg) were amplified with the QuantiTect SYBER Green PCR Kit (Qiagen, Osaka, Japan) under the following conditions: initial denaturation for 10 min at 94°C followed by 40 cycles consisting of 15 s at 94°C and 1 min at 60°C. The data analysis consisted of a fold induction, and the expression ratio was calculated from the differences in the threshold cycles at which an increase in the reporter fluorescence above a baseline signal could first be detected among the three samples and was averaged for duplicate experiments. The sequence of primers we utilized in the real-time PCR to detect human Col2A1 and human GAPDH were: hCol2A1 forward 5′-GAGT CAAGGGTGATCGTGGT-3′, reverse 5′-CACCTTGG TCT CCAGAAGGA-3′; hGAPDH forward 5′-GAAGG TGAAGGTCGGAGTCA-3′, reverse 5′-GAAGATGGT GATGGGATTTC-3′. hGAPDH was used as a housekeeping gene.

RESULTS

Proliferation of Auricular or Costal Chondrocytes With or Without FBS

In a microtia operation, both remnant auricular cartilage and surgical debris of the costal cartilage, neither of which is used for reconstructive surgery, were obtained from individual patients. The mean weight was 1.18 g (1.00–1.42, $n = 5$) or 3.60 g (2.2–5.0, $n = 5$), respectively, while the mean cell number of the isolated chondrocytes was 3.8×10^6 (1.5×10^6–7.0×10^6) or 2.5×10^6 (1.0×10^6–4.0×10^6). We first examined the proliferation of the auricular and costal chondrocytes taken from these tissues. When the commercial medium, CGM containing 5% FBS with an undisclosed concentration of FGF-2, IGF-I, and insulin, was used for chondrocyte proliferation and passage was performed every week, both kinds of chondrocytes showed exponential growth after some lag phase in all five patients. The growth rate was higher in the auricular chondrocytes than in costal ones. Figure 1 shows the typical growth curve of two patients. The auricular chondrocytes increased their number by 1000-fold within passages 3–4 (3–4 weeks), while it took more than five passages (5 weeks) for the costal ones (Fig. 1).

Next, we attempted to substitute FBS for HS and/or some other factors. When we examined the proliferation of the auricular chondrocytes in the medium without any serum or soluble factors, they did not undergo proliferation at all (Fig. 2, open bar). When we added FGF-2 and IGF-I, whose combination had been known to increase the proliferation in a previous paper (42), little proliferation was noted (Fig. 2, open bar). In contrast, HS may have some effects on the proliferation of auricular chondrocytes, but it provided no more than twofold in 2 weeks (Fig. 2, filled bar). FBS showed better proliferation of approximately threefold within 2 weeks (Fig. 2, filled bar). When FGF-2 and IGF-I were added to the medium containing HS or FBS, the proliferation was increased to approximately seven- to ninefold in both (Fig 2, slanted striped bars), suggesting the possibility that HS may promote proliferation to the same extent as FBS, with some soluble factors. However, none of them were over that of CGM (Fig. 2, horizontal striped bar).

Statistical Analysis for Combinational Effects of Soluble Factors

We selected 12 kinds of soluble factors to be examined (Table 1). We used a fractional factorial design to determine an optimal combination with a minimal number of experiments. Using 256 kinds of media determined by the software JMP-5.1.1.J (Table 2), we examined the proliferation effects in a colorimetric assay. The results obtained for the 256 kinds of media were also analyzed by the software JMP-5.1.1.J.

In this analysis, FGF-2, Dex, insulin, and IGF-I showed parameter estimates of 0.192 ($F = 676$), 0.0943 ($F = 166$), 0.0626 ($F = 75.1$), and 0.0524 ($F = 52.6$), respectively, and they showed significant effects on proliferation alone ($p < 0.001$). Eight other factors did not prominently promote proliferation of the auricular chondrocytes in the presence of 5% HS, and especially BMP-2 worked rather negatively in the chondrocyte proliferation (parameter estimate −0.194, $F = 720$). Regarding synergy, the interaction term of FGF-2 and insulin and that of FGF-2 and IGF-I exhibited statistically positive effects (parameter estimates 0.0582 and 0.0565, $F = 64.3$ and 60.7, $p < 0.001$), although IGF-I and insulin decreased the effects of synergy (parameter estimate −0.0601, $F = 68.7$, $p < 0.001$). Therefore, we chose the combinations of FGF-2 with insulin or IGF-I as ideal ones that showed high F-values in both individual factors and interaction terms of two factors. Actually, the combinations of FGF-2 and insulin or FGF-2 and IGF-I showed high values of parameter estimates, suggesting strong effects on proliferation, when the chondrocytes were cultured together with 5% HS (Fig. 3).

Effects of Doses of FGF-2, Insulin, and IGF-I on the Synergy

To confirm the effects of FGF-2, insulin, IGF-I, or their combinations on chondrocyte proliferation, the increase in cell numbers was counted, following the culture in the media containing 5% HS with those factors

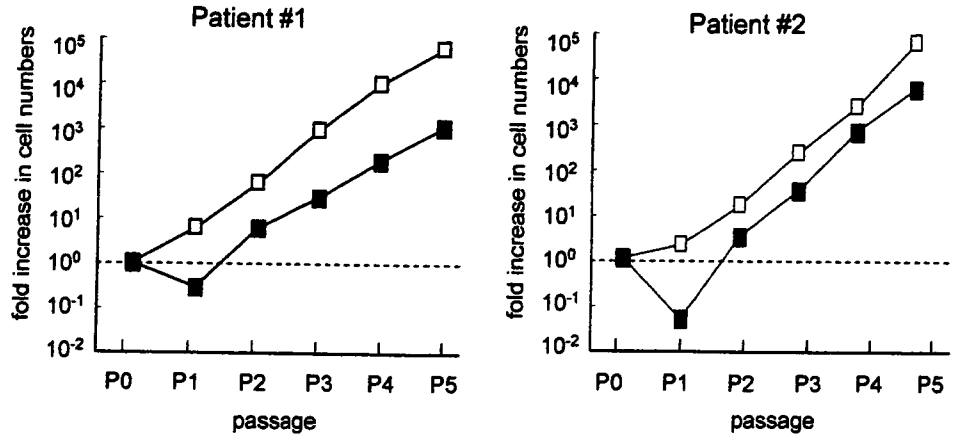

Figure 1. Growth curves of human chondrocytes. Each kind of cell was cultured in a six-well plate with CGM. Every week, the cells were harvested, counted in numbers, and reseeded in a six-well plate until the cell numbers increased more than 1000-fold. The number of auricular chondrocytes (open square) arrived at a 1000-fold increase more quickly than that of the costal cartilage (filled square) in all patients ($n = 5$).

or their combination in various doses. FGF-2 showed a dose dependency for proliferation in the range of 10–500 ng/ml, although more than 1 μg /ml seemed to be the top limit. Insulin and IGF-I did not exhibit increasing effects on proliferation in the range of 5–500 μg/ml or 100 ng–10 μg/ml, respectively (Fig. 4).

The synergistic effects of insulin or IGF-I with FGF-2 seemed to be maintained until the dose of FGF-2 increased to 100 ng/ml (Fig. 5). In the combination of 10 ng/ml FGF-2 with 5 μg/ml insulin or 100 ng/ml IGF-I, the cell number increased to approximately 12- or 10-fold, respectively, within 2 weeks, while the increase was limited to eightfold with FGF-2 alone (Fig. 5, FGF-2 10 ng/ml). The addition of both insulin and IGF-I to FGF-2 showed an 11-fold increase, which was somewhat lower, compared with the combination of FGF-2 with insulin (12-fold) (Fig. 5, FGF-2 10 ng/ml). The same tendency was observed in the combination of 100 ng/ml FGF-2 with insulin, IGF-I, or both. Especially the combination of 100 ng/ml FGF-2 and insulin showed prominent proliferation (16-fold) (Fig. 5, FGF-2 100 ng/ml). When the dose of FGF-2 was 500 ng/ml, the addition of insulin, IGF-I, or both made little difference compared with FGF-2 alone, suggesting that synergistic effects of insulin and IGF-I were not found at this dose of FGF-2 (Fig. 5, FGF-2 500 ng/ml). Although 500 ng/

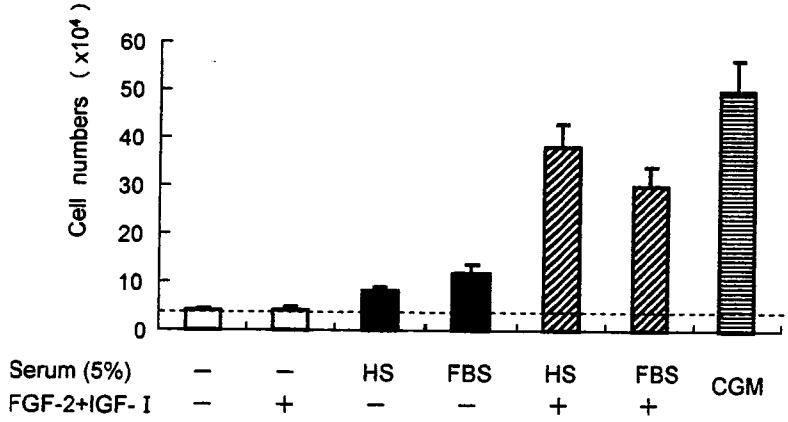

Figure 2. Effects of FBS, HS, or additional soluble factors on the chondrocyte proliferation. Human auricular chondrocytes (2×10^4 cells corresponding to the broken line) obtained from five patients were encapsulated in 2 ml of atelocollagen gel and incubated with each kind of medium in a six-well plate for 2 weeks ($n = 5$ for each medium). HS, human serum; FBS, fetal bovine serum; FGF-2, 10 ng/ml; IGF-I, 100 ng/ml. All values are presented as mean + SD.

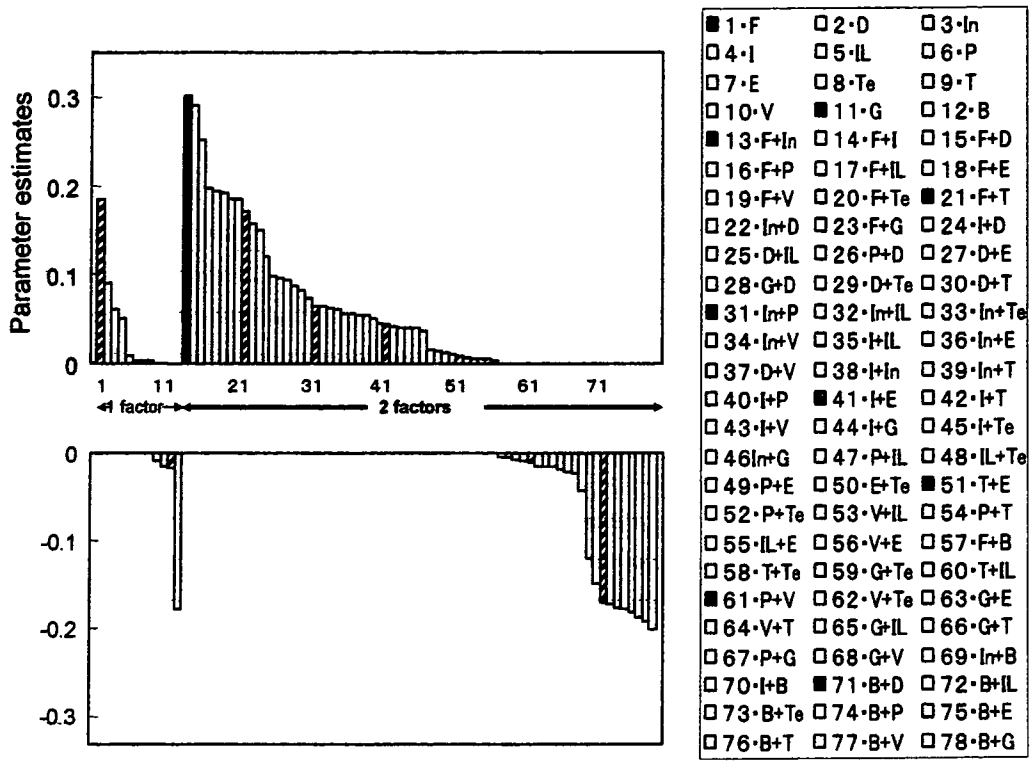

Figure 3. Results of analysis of variance by fractional factorial design. FGF-2 (column #1), Dex (column #2), insulin (column #3), and IGF-I (column #4) showed high values of parameter estimates, suggesting the promotion of proliferation. The combination of FGF-2 and insulin (column #13) and that of FGF-2 and IGF-I (column #14) were strongly effective for proliferation. However, the simultaneous use of insulin and IGF-I (column #38) somewhat decreased the effects of synergy, compared with a single use of insulin (column #3) or IGF-I (column #4). F, FGF-2; D, Dex; In, insulin; I, IGF-I; IL, IL-1RA; P, PTH; E, E_2; Te, testosterone; T, T3; V, vitD; G, GH; B, BMP-2.

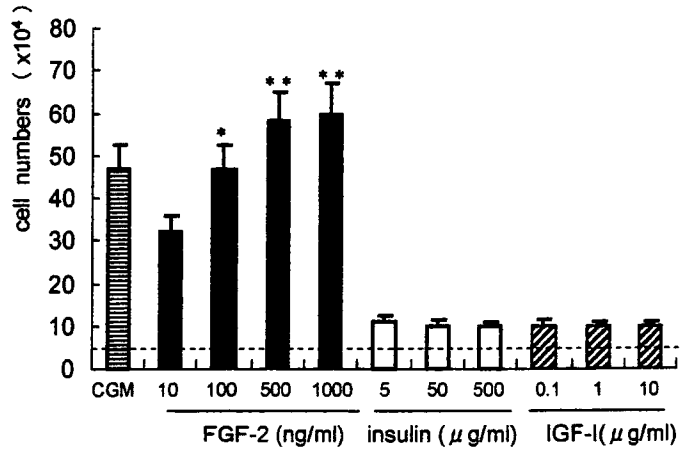

Figure 4. Dose dependency of FGF-2, insulin, and IGF-I in the chondrocyte proliferation. Human auricular chondrocytes were 3D cultured in the media containing DMEM/F-12 with 5% HS and FGF-2, insulin, or IGF-I at various kinds of doses for 2 weeks ($n = 5$ for each medium). All values are presented as mean + SD. Statistics were assessed using the Student's t-test (*$p < 0.05$ vs. FGF-2 10 ng/ml, **$p < 0.05$ vs. FGF-2 100 ng/ml). The broken line indicates the number of chondrocytes at the starting point of incubation (2×10^4 cells).

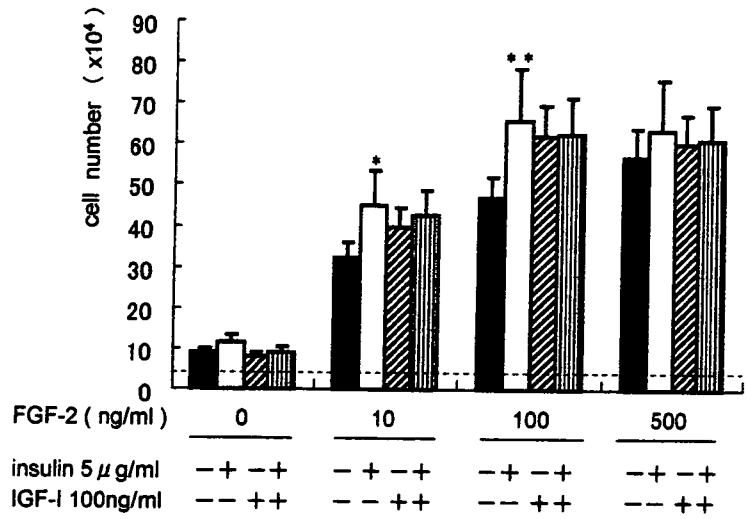

Figure 5. Synergistic effects of FGF-2 with insulin or IGF-I on the chondrocyte proliferation. The cell numbers of human auricular chondrocytes from the different patients were counted after a 2-week incubation ($n = 5$ for each medium). The media contained DMEM/F-12 with 5% HS and the soluble factors. The broken line indicates the initial number of chondrocytes at the starting point (2×10^4 cells). All values are presented as mean + SD. Statistics were assessed using the Student's t-test (*$p < 0.05$ vs. the group using FGF-2 10 ng/ml alone, **$p < 0.05$ vs. the group using FGF-2 100 ng/ml alone).

ml of FGF-2 alone showed higher proliferation effects than did 100 ng/ml, the combinations of 500 ng/ml FGF-2 with insulin, IGF-I, or both showed almost the same proliferation ability as those combinations with 100 ng/ml FGF-2 (Fig. 5). These results were reproducible in every lot of HS (data not shown).

To confirm the actual 1000-fold increase in the cell numbers, we examined a long-term culture with repeated passaging of the auricular chondrocytes in 5% HS-DMEM/F-12 containing FGF-2 (100 ng/ml) with or without insulin (5 μg/ml) or IGF-I (100 ng/ml). A passage was performed every other week, an interval that corresponded to the period used in the above experiments for determining the kinds and doses of the soluble factors. In the growth curves, all kinds of media as well as the CGM provided good proliferation after some lag phase, and realized a 1000-fold increase during passage 4 (Fig. 6). Especially, the combination of FGF-2 and insulin exhibited the highest growth rate, arriving at 10,000-fold within passage 4.

Finally, we checked the gene expression pattern of the chondrocytes proliferated in these four kinds of media. All of them showed an absolutely lower expression in Col2A1, compared with chondrocytes of the primary culture (passage 0). The expression ratio was 7470 ± 2450 in the primary culture, while those of a long-term culture in CGM, the medium containing FGF-2, and that in the combination of FGF-2 with insulin or IGF-I were 2.96 ± 1.82, 7.26 ± 4.59, 11.3 ± 7.11, and 15.5 ± 3.50, respectively.

DISCUSSION

The first issue that we must achieve is to gain sufficient cell numbers of cultured chondrocytes for the cartilage regenerative medicine. A previous report described that fetal elastic chondrocytes proliferated more quickly than fetal hyaline cartilage (9). In the present study, the auricular chondrocytes of school children age patients also had more favorable proliferation, compared with the costal ones. In addition, we could determine an effective proliferation medium containing human serum or several soluble factors, showing high responsiveness to the auricular chondrocytes. Also because the auricular cartilage can be accessed easily in minimally invasive fashion, through a simple auricle biopsy, this kind of chondrocyte would be a good candidate for a cell source for cartilage regenerative medicine.

In the present study, we determined the combinations of two factors, which promote the proliferation of human auricular chondrocyte in the presence of 5% HS, among 12 soluble factors, by analysis of variance in fractional factorial design. For the analysis, we did not confine the factors to be examined to those that had been previously published to be effective for the proliferation of the human auricular chondrocytes, but used many factors that are reported to possess some effects on either

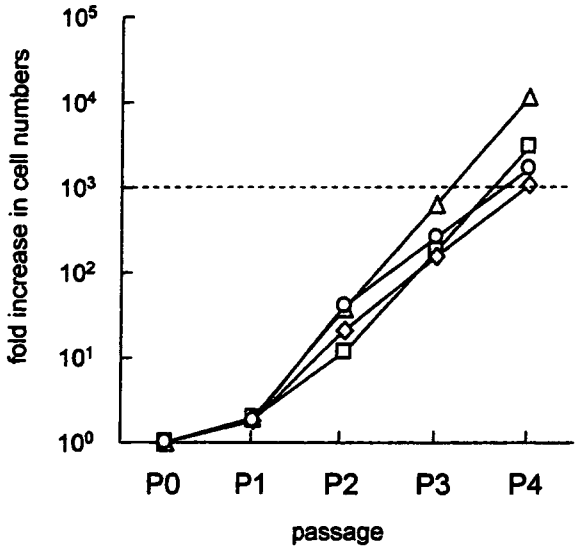

Figure 6. Growth curves of human auricular chondrocytes cultured in various kinds of media. Passage was performed every other week. DMEM/F-12 containing 5% HS with 100 ng/ml FGF-2 and 5 μg/ml insulin (triangles) provided more than a 10,000-fold increase during passage 4, while CGM (squares) and DMEM/F-12 containing 5% HS with FGF-2 alone (diamonds) or the combination of FGF-2 and IGF-I (circles) also arrived at 1000-fold during passage 4.

the proliferation or differentiation of chondrocytes, including those derived from animals and cell lines in order to widen the screening size. The doses of each soluble factor were those used in previous studies (Table 1).

We confirmed the synergistic effects of FGF-2 with insulin or IGF-I in the human auricular chondrocytes and proved their usefulness in combination with HS. Although it is well known that FGF-2, insulinm and IGF-I are mitogenic to chondrocytes (13,14,30), the mechanisms that promote chondrocyte proliferation seem to be different among such mitogens. Bohme and collaborators reported that insulin or IGF-1 could trigger chondrocyte proliferation under strictly serum-free conditions, although FGF-2 did not promote cell division in serum-free cultures of chondrocytes (3). Quarto and coworkers also described that FGF-2 alone does not induce cell proliferation of chick embryonic chondrocytes without FBS (24). In contrast, FGF-2 could bolster the mitogenic activity of FBS in cultures, indicating that the cells became conditioned by FBS so that they could respond to FGF-2 (3).

This difference in the conditions in which each factor expresses mitogenic activity may be explained by the general concept of competence and progression factors, both of which are required to trigger cell division. The former include FGF-2, EGF, or PDGF, allowing the passage from G_0 to G_1 at the entry in the cell cycle, while the latter correspond to insulin or IGF-I, which commit the cells to DNA synthesis (1). The synergy of FGF-2 with insulin or IGF-I seemed to be associated with the cooperation of these competence and progression factors. In contrast, because insulin and IGF-I, which possess a common role as progression factors, did not compensate each other and could not accelerate the cell cycle effectively, the simultaneous use of both insulin and IGF-I did not help the promotion of proliferation, as seen in the present study. Further studies on signal pathways downstream of FGF-2 and insulin or IGF-I in chondrocytes are anticipated to disclose not only the detailed mechanisms of the synergistic effects of those factors but also to provide the optimal promotion of chondrocyte proliferation.

In contrast, BMP-2 worked rather negatively in the chondrocyte proliferation. In the experiment using the murine chondrocytic cell line ATDC5, BMP-2 upregulated the expression of the type II and type X collagen mRNA and stimulated the sequential progression of the early and late phase differentiation, although it had little effect on the proliferation of the cells (27). Also, for human auricular chondrocytes, BMP-2 is speculated to drive the direction to produce the cartilaginous matrix, but to arrest the progression of the cell cycles.

Regarding the doses of FGF-2, less than 10 ng/ml was used for the promotion of proliferation in chondrocytes and MSC in many previous reports (13,25,28). Quatela and collaborators did not show that doses of FGF-2 greater than 100 ng/ml provide increasing effects on proliferation of human auricular chondrocytes in monolayer culture (25). Because the capacity of a 3D culture system for cells is higher than that in a monolayer culture, even more than 100 ng/ml FGF-2 continues to promote chondrocyte proliferation and maintain the synergistic effects with insulin or IGF-I, as seen in the present data.

After the long-term culture, which provided more than a 1000-fold increase in cell numbers, any kind of media we examined equivalently brought dedifferentiation of the chondrocytes. Chondrocytes embedded in native tissue synthesize type II collagen and proteoglycan, although the same cells cultured in a monolayer lose their typical morphology from round to a spindle fibroblast-like shape and protein synthesis, a phenomenon termed dedifferentiation (29). In order to reverse this inevitable phenomenon, many researchers have used 3D culture embedded in agarose gel (2), alginate beads (4), collagen type I gel (15), or collagen type II gel (16). However, when we applied the 3D embedded culture for chondrocyte proliferation, mRNA expression of the proliferated chondrocytes showed a dedifferentiation

pattern that the Col2a1 expression decreased, compared with those of the primary culture of the chondoryctes. It suggested that dedifferentiation inevitably occurs, even if it may be less in the 3D-embedded culture than in the monolayer culture, when the period of cell culture becomes long. Therefore, when we obtain a sufficient number of cells after a long proliferation culture, we should change the culture system, including the medium contents or cell density, in order to reverse the dedifferentitaion. At present, we have investigated the optimal medium inducing redifferentiation of the chondoryctes, and realized the production of regenerated cartilage possessing mature and abundant cartilaginous matrix in vitro.

ACKNOWLEDGMENTS: Funding for this research was provided by Grants-in-Aid for Scientific Research from the Japanese Ministry of Education, Culture, Sports, Science and Technology (#15390539, #16390431, and #16659546), Daiwa Securities Health Foundation, and Research Society for Metabolic Bone Diseases.

REFERENCES

1. Aaronson, S. A. Growth factors and cancer. Science 254: 1146–1153; 1991.
2. Benya, P. D.; Shaffer, J. D. Dedifferentiated chondrocytes reexpress the differentiated collagen phenotype when cultured in agarose gels. Cell 30:215–224; 1982.
3. Bohme, K.; Conscience-Egli, M.; Tschan, T.; Winterhalter, K. H.; Bruckner, P. Induction of proliferation or hypertrophy of chondrocytes in serum-free culture: The role of insulin-like growth factor-I, insulin, or thyroxine. J. Cell Biol. 116:1035–1042; 1992.
4. Bonaventure, J.; Kadhom, N.; Cohen-Solal, L.; Ng, K. H.; Bourguignon, J.; Lasselin, C.; Freisinger, P. Reexpression of cartilage-specific genes by dedifferentiated human articular chondrocytes cultured in alginate beads. Exp. Cell Res. 212:97–104; 1994.
5. Brittberg, M.; Lindahl, A.; Nilsson, A.; Ohlsson, C.; Isaksson, O.; Peterson, L. Treatment of deep cartilage defects in the knee with autologous chondrocyte transplantation. N. Engl. J. Med. 331:889–895; 1994.
6. Caldamone, A. A.; Diamond, D. A. Long-term results of the endoscopic correction of vesicoureteral reflux in children using autologous chondrocytes. J. Urol. 165:2224–2227; 2001.
7. Choi, Y. C.; Morris, G. M.; Lee, F. S.; Sokoloff, L. The effect of serum on monolayer cell culture of mammalian articular chondrocytes. Connect. Tissue Res. 7:105–112; 1980.
8. Finney, D. J. The fractional replication of factorial arrangements. Ann. Eugenics 12:291–301; 1945.
9. Fuchs, J. R.; Terada, S.; Hannouche, D.; Ochoa, E. R.; Vacanti, J. P.; Fauza, D. O. Engineered fetal cartilage: Structural and functional analysis in vitro. J. Pediatr. Surg. 37:1720–1725; 2002.
10. Glaser, J. H.; Conrad, H. E. Properties of chick embryo chondrocytes grown in serum-free medium. J. Biol. Chem. 259:6766–6772; 1984.
11. Grigoriadis, A. E.; Aubin, J. E.; Heersche, J. N. Effects of dexamethasone and vitamin D3 on cartilage differentiation in a clonal chondrogenic cell population. Endocrinology 125:2103–2110; 1989.
12. Johnson, L. F.; deSerres, S.; Herzog, S. R.; Peterson, H. D.; Meyer, A. A. Antigenic cross-reactivity between media supplements for cultured keratinocyte grafts. J. Burn Care Rehabil. 12:306–312; 1991.
13. Kamil, S. H.; Aminuddin, B. S.; Bonassar, L. J.; Silva, C. A.; Weng, Y.; Woda, M.; Vacanti, C. A.; Eavey, R. D.; Vacanti, M. P. Tissue-engineered human auricular cartilage demonstrates euploidy by flow cytometry. Tissue Eng. 8:85–92; 2002.
14. Kato, Y.; Gospodarowicz, D. Growth requirements of low-density rabbit costal chondrocyte cultures maintained in serum-free medium. J. Cell Physiol. 120:354–363; 1984.
15. Kimura, T.; Yasui, N.; Ohsawa, S.; Ono, K. Chondrocytes embedded in collagen gels maintain cartilage phenotype during long-term cultures. Clin. Orthop. 186:231–239; 1984.
16. Malemud, C. J.; Stevenson, S.; Mehraban, F.; Papay, R. S.; Purchio, A. F.; Goldberg, V. M. The proteoglycan synthesis repertoire of rabbit chondrocytes maintained in type II collagen gels. Osteoarthritis Cartilage 2:29–41; 1994.
17. Malinin, T. I.; Hornicek, F. J. Response of human chondrocytes cultured in vitro to human somatotropin, triiodothyronine, and thyroxine. Transplant. Proc. 29:2037–2039; 1997.
18. Maor, G.; Segev, Y.; Phillip, M. Testosterone stimulates insulin-like growth factor-I and insulin-like growth factor-I-receptor gene expression in the mandibular condyle—a model of endochondral ossification. Endocrinology 140: 1901–1910; 1999.
19. Meyer, A. A.; Manktelow, A.; Johnson, M.; deSerres, S.; Herzog, S.; Peterson, H. D. Antibody response to xenogeneic proteins in burned patients receiving cultured keratinocyte grafts. J. Trauma 28:1054–1059; 1988.
20. Monsonego, E.; Halevy, O.; Gertler, A.; Hurwitz, S.; Pines, M. Growth hormone inhibits differentiation of avian epiphyseal growth-plate chondrocytes. Mol. Cell. Endocrinol. 114:35–42; 1995.
21. Mushtaq, T.; Farquharson, C.; Seawright, E.; Ahmed, S. F. Glucocorticoid effects on chondrogenesis, differentiation and apoptosis in the murine ATDC5 chondrocyte cell line. J. Endocrinol. 175:705–713; 2002.
22. Ochi, M.; Uchio, Y.; Kawasaki, K.; Wakitani, S.; Iwasa, J. Transplantation of cartilage-like tissue made by tissue engineering in the treatment of cartilage defects of the knee. J. Bone Joint Surg. Br. 84:571–578; 2002.
23. Peterson, L.; Minas, T.; Brittberg, M.; Lindahl, A. Treatment of osteochondritis dissecans of the knee with autologous chondrocyte transplantation: Results at two to ten years. J. Bone Joint Surg. Am. 85A:17–24; 2003.
24. Quarto, R.; Campanile, G.; Cancedda, R.; Dozin, B. Modulation of commitment, proliferation, and differentiation of chondrogenic cells in defined culture medium. Endocrinology 138:4966–4976; 1997.
25. Quatela, V. C.; Sherris, D. A.; Rosier, R. N. The human auricular chondrocyte. responses to growth factors. Arch. Otolaryngol. Head Neck Surg. 119:32–37; 1993.
26. Rodd, C.; Jourdain, N.; Alini, M. Action of estradiol on epiphyseal growth plate chondrocytes. Calcif. Tissue Int. 75:214–224; 2004.
27. Shukunami, C.; Ohta, Y.; Sakuda, M.; Hiraki, Y. Sequen-

tial progression of the differentiation program by bone morphogenetic protein-2 in chondrogenic cell line ATDC5. Exp. Cell Res. 241:1–11; 1998.
28. Tsutsumi, S.; Shimazu, A.; Miyazaki, K.; Pan, H.; Koike, C.; Yoshida, E.; Takagishi, K.; Kato, Y. Retention of multilineage differentiation potential of mesenchymal cells during proliferation in response to FGF. Biochem. Biophys. Res. Commun. 288:413–419; 2001.
29. von der Mark, K.; Gauss, V.; von der Mark, H.; Muller, P. Relationship between cell shape and type of collagen synthesised as chondrocytes lose their cartilage phenotype in culture. Nature 267:531–532; 1977.
30. Wroblewski, J.; Edwall-Arvidsson, C. Inhibitory effects of basic fibroblast growth factor on chondrocyte differentiation. J. Bone Miner. Res. 10:735–742; 1995.
31. Yasuda, T.; Poole, A. R. A fibronectin fragment induces type II collagen degradation by collagenase through an interleukin-1-mediated pathway. Arthritis Rheum. 46:138–148; 2002.
32. Zerega, B.; Cermelli, S.; Bianco, P.; Cancedda, R.; Cancedda, F. D. Parathyroid hormone [PTH(1-34)] and parathyroid hormone-related protein [PTHRP(1-34)] promote reversion of hypertrophic chondrocytes to a prehypertrophic proliferating phenotype and prevent terminal differentiation of osteoblast-like cells. J. Bone Miner. Res. 14:1281–1289; 1999.

Light-induced gene transfer from packaged DNA enveloped in a dendrimeric photosensitizer

NOBUHIRO NISHIYAMA[1]*, AYA IRIYAMA[2]*, WOO-DONG JANG[3], KANJIRO MIYATA[3], KEIJI ITAKA[1], YUJI INOUE[2], HIDENORI TAKAHASHI[2], YASUO YANAGI[2], YASUHIRO TAMAKI[2], HIROYUKI KOYAMA[4] AND KAZUNORI KATAOKA[1,3]†

[1]Center for Disease Biology and Integrative Medicine, Graduate School of Medicine, The University of Tokyo, 7-3-1 Hongo, Bunkyo-ku, Tokyo 113-0033, Japan
[2]Department of Ophthalmology, University of Tokyo Hospital, 7-3-1 Hongo, Bunkyo-ku, Tokyo 113-8655, Japan
[3]Department of Materials Engineering, Graduate School of Engineering, The University of Tokyo, 7-3-1 Hongo, Bunkyo-ku, Tokyo 113-8656, Japan
[4]Department of Clinical Vascular Regeneration, The University of Tokyo Hospital, 7-3-1 Hongo, Bunkyo-ku, Tokyo 113-8655, Japan
*These authors contributed equally to this paper
†e-mail: kataoka@bmw.t.u-tokyo.ac.jp

Published online: 20 November 2005; doi:10.1038/nmat1524

The control of gene transfection in the body is a core issue in gene therapy. Photochemical internalization is a technology that allows light-induced delivery of DNA, drugs or other biological factors directly inside cells. Usually it requires that a photosensitizer be added to the drug-delivery system to photochemically destabilize the endosomal membrane. Here we present a system for *in vivo* DNA delivery in which these two components are assembled into one structure. This is a ternary complex composed of a core containing DNA packaged with cationic peptides and enveloped in the anionic dendrimer phthalocyanine, which provides the photosensitizing action. The ternary complex showed more than 100-fold photochemical enhancement of transgene expression *in vitro* with reduced photocytotoxicity. In an animal experiment, subconjuctival injection of the ternary complex followed by laser irradiation resulted in transgene expression only in the laser-irradiated site. This work demonstrates a new biomedical application for dendrimers, and the first success in the photochemical-internalization-mediated gene delivery *in vivo*.

There has been a strong incentive for the development of safe and effective gene vectors to achieve successful *in vivo* gene therapy[1–4]. Compared with viral vectors with an inherent risk for clinical use, non-viral synthetic vectors have received much attention owing to the advantages of safety, simplicity of use and ease of mass production[1–4]. A promising approach to the design of synthetic vectors is the use of cationic polymers and peptides. In general, the plasmid DNA (pDNA)/polycation complexes (polyplexes) are internalized by the cell through the endocytic pathway and need to be released from the endosome to deliver the genes to the nucleus. It is well known that this endosomal escape of the polyplexes is the main obstacle to obtaining efficient transfection[5]. Polycations possessing a buffering capacity, such as polyethylenimine (PEI), show a high *in vitro* transfection activity owing to the so-called proton sponge effect[5]; however, it is probable that the inherent cytotoxicity will impair their clinical utility as gene carriers. Hence, further efforts need to be devoted to the development of synthetic vectors especially for *in vivo* use.

In contrast, site-specific gene transfer to somatic cells is strongly desired; however, the existing vectors, including the viral and non-viral vectors, might have great difficulty in achieving *in vivo* transfection in a site-specific manner. In this regard, a different concept has been proposed[6–10], photochemical internalization (PCI): the cytoplasmic delivery of macromolecular compounds is enhanced by the photochemical disruption of the endosomal membrane using light and a hydrophilic photosensitizer. This smart concept is, in principle, applicable to the *in vivo* gene delivery in a light-sensitive manner[10]. However, the cytotoxicity is accompanied by photochemical reactions in the cell, and this might need to be reduced before considering further applications of this technology. Moreover, there is still room for optimization and modification

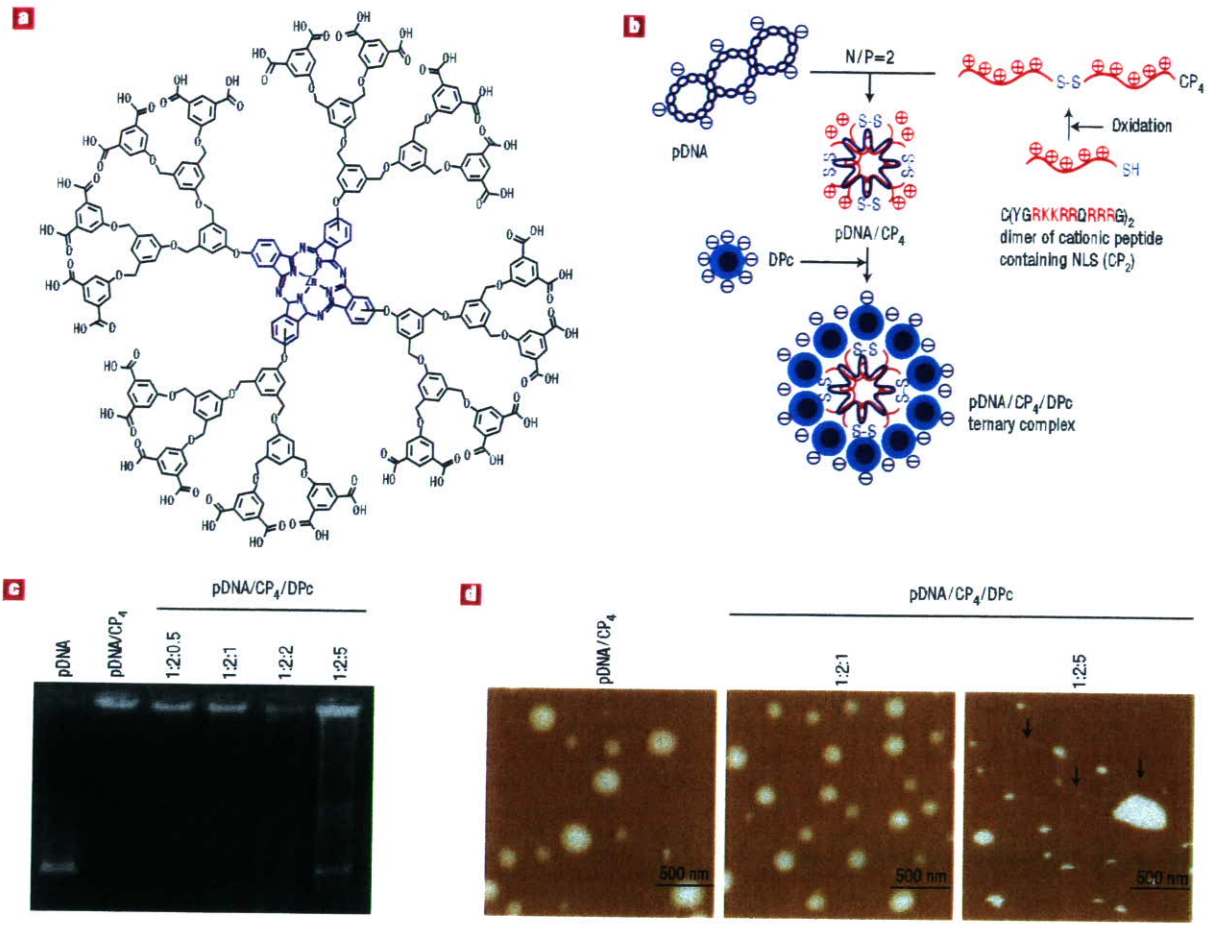

Figure 1 Preparation and characterization of the ternary complex. a, The chemical structure of ionic DPc. **b**, A scheme for preparation of the pDNA/CP_4/DPc ternary complex. **c**, Gel retardation assay of the pDNA/CP_4 polyplex prepared at an N/P ratio of 2, and the ternary complexes with varying charge molar ratios of pDNA/CP_4/DPc. **d**, AFM images of the pDNA/CP_4 and pDNA/CP_4/DPc complexes. Arrow heads indicate plasmid DNA released from the ternary complexes.

for *in vivo* applications. From the viewpoint of materials science, this concept can be integrated into nanodevices for drug and gene delivery.

In the present paper, we assume that the control of subcellular localization of photosensitizers may be a key to the PCI-mediated gene delivery with reduced cytotoxicity, because the photodamage to sensitive organelles other than the endosomal membrane, for example the plasma and mitochondrial membranes, might be responsible for the photocytotoxicity[11]. In addition, gene carriers should be equipped with a photosensitizing unit as one component for *in vivo* applications. These assumptions motivated us to develop a light-responsive gene carrier based on a ternary complex of pDNA, cationic peptides and anionic dendrimer-based photosensitizers (dendrimer phthalocyanine: DPc; Fig. 1a). Dendrimers, the three-dimensional tree-like branched macromolecules, have attracted growing interest as materials for drug and gene delivery[12–16], and the ternary complex is a different biomedical application of dendrimers. The ternary complex has shown significant photochemical enhancement of the transgene expression *in vitro* with reduced photocytotoxicity and *in vivo* gene transfer to the conjunctival tissue in the rat eye in a light-selective manner.

The ternary complex is composed of a core of a pDNA/cationic polymer polyplex enveloped with anionic DPc (Fig. 1a) as illustrated in Fig. 1b. DPc possesses a centre phthalocyanine molecule surrounded by a second generation of aryl ether dendrons, and 32 carboxyl groups on the periphery of DPc allow polyion complex formation with cationic polyplexes. In the present study, the core polyplex was formed from a quadruplicated cationic peptide (CP_4), where a peptide (CP_2: C(YGRKKRRQRRRG)$_2$)) was dimerized through a disulphide linkage, and pDNA was mixed with the CP_4 peptide at a molar ratio of cationic amino acids to a phosphate anion in DNA (N/P ratio) of 2. It has been demonstrated[17] that CP_2 and CP_4 contain a nuclear localization sequence (NLS) and thereby effectively mediate the gene transfection to the cell with the aid of conventional transfection reagents such as PEI and LipofectAMINE to promote the endosomal escape of the polyplex. Thus, these potent cationic peptides were used for the formation of the ternary complex to ensure the efficient gene transfection following the endosomal escape of the polyplex.

In this study, the ternary complexes were prepared by varying the charge molar ratios of pDNA/CP_4/DPc, and the complex formation was confirmed by a gel retardation assay (Fig. 1c). As a result, pDNA was incorporated into the complexes with charge ratios up to 1:2:2, but was excluded from the complex with a charge ratio of 1:2:5. The release of pDNA from the 1:2:5 complex was also observed by atomic force microscopy (AFM) as shown in Fig. 1d.

Table 1 Size, size distribution and ζ-potential of the electrostatic assemblies containing plasmid DNA.

	Cumulant diameter (nm)	Polydispersity index	ζ-potential (mV)
pDNA/PEI (1:10)	127.8	0.211	23.8±0.1
pDNA/CP_4 (1:2)	100.8	0.185	21.3±2.3
pDNA/CP_4/DPc (1:2:0.5)	149.7	0.115	−8.5±3.6
pDNA/CP_4/DPc (1:2:1)	130.8	0.108	−29.2±2.6
pDNA/CP_4/DPc (1:2:2)	107.7	0.143	−23.2±0.9
pDNA/CP_4/DPc (1:2:5)	267.1	0.180	−49.6±0.7
pDNA/CP_4/PAA* (1:2:0.5)	621.2	0.444	−27.1±0.8
pDNA/CP_4/PAA (1:2:1)	672.0	0.477	−25.8±0.4
pDNA/CP_4/PAA (1:2:2)	912.3	0.361	−24.3±0.8
pDNA/CP_4/PAA (1:2:5)	1426	0.278	−25.3±2.3

* PAA: Poly(aspartic acid) homopolymer with a polymerization degree of 26

Thus, addition of excess DPc might disintegrate the pDNA/CP_4 polyplex. The size, polydispersity index and ζ-potential of the pDNA/CP_4/DPc ternary complexes are summarized in Table 1. The addition of DPc to the positively charged pDNA/CP_4 polyplex gave negative ζ-potential values, suggesting the formation of ternary complexes covered with anionic DPc. A decrease in the size of the ternary complexes with increasing DPc ratios may be attributed to shrinkage of the cationic peptide corona on the polyplex surface through electrostatic interaction with DPc. Surface modification with anionic DPc provided the 1:2:1 and 1:2:2 complexes with excellent colloidal stability, whereas the 1:2:0.5 complex possessing an almost neutral ζ-potential value tended to precipitate in several hours. Significantly, the ternary complexes showed much lower polydispersity indices compared with the pDNA/CP_4 or PEI polyplexes (Table 1). The AFM observation has revealed consistently that the 1:2:1 complex consists of spherical particles with a narrow size distribution, which is in marked contrast to the pDNA/CP_4 polyplex containing large aggregates (Fig. 1d). Note that the addition of poly(aspartic acid) (PAA) homopolymer with a polymerization degree of 26 to the pDNA/CP_4 polyplex resulted in a large aggregate formation (Table 1). Hence, the three-dimensional structure of DPc is assumed to play an essential role in the formation of a ternary complex with a narrow size distribution and excellent colloidal stability. The layer-by-layer assemblies of oppositely charged polyelectrolytes onto colloidal particles have attracted considerable attention[18,19]; however, the pDNA/CP_4/DPc ternary complex is definitely discriminated from the layer-by-layer assemblies, because a core composed of hard materials is not required for the formation of the ternary complex. Thus, the ternary complex presented here is a supramolecular assembly consisting of a pDNA/CP_4 polyplex core and a DPc envelope.

The properties of DPc and the ternary complex related to the initial steps in the gene transfection to the cell (that is, processes from the cellular uptake to when photodamage to the endosomal membrane occurred) were evaluated, because the ternary complex was designed to control these processes. First, the cellular uptake of the ternary complex was evaluated by flow cytometry using a fluorescein-labelled pDNA, as shown in Fig. 2a. The amount of cellular uptake of the ternary complexes was less than that of cationic polyplexes such as pDNA/CP_4 and pDNA/PEI, and decreased as the DPc ratio increased. The ternary complex covered with anionic DPc should have a lower affinity for the negatively charged plasma membrane of cells, accounting for the results in Fig. 2a.

The pH-dependent hydrophilic/hydrophobic behaviour of DPc and its possible interaction with cell membranes was estimated by octanol/water partitioning, which is a common method for evaluation of drug–membrane interactions[20]. The partitioning (%) of DPc to the octanol phase increased as the pH decreased to 5.0–5.5 (Fig. 2b), suggesting the increased hydrophobicity of DPc and possible interactions with cell membranes under low-pH conditions. Because the DPc consists of a hydrophobic dendritic framework, the protonation of the peripheral carboxyl group under acidic conditions might increase its hydrophobicity. This result suggests that DPc may be released from the ternary complex under endosomal pH conditions to interact with the endosomal membrane, while electrostatically interacting with the positively charged surface of the polyplex at physiological pH. This assumption offers an interesting opportunity to selectively photodamage the endosomal membrane for effective PCI.

Figure 2c shows the subcellular distribution of FITC-labelled dextran co-incubated with the 1:2:1 ternary complex. It was demonstrated that FITC-dextran showed diffused fluorescence throughout the cytoplasm after photoirradiation, whereas it showed punctuated fluorescence corresponding to localization in the endosome and/or lysosome before photoirradiation. This result suggests the capability of the ternary complex of releasing the contents in the vesicular organelles to the cytoplasm on photoirradiation.

To evaluate the potential of the ternary complex for PCI-mediated gene delivery, *in vitro* transfection experiments were performed on HeLa cells with a luciferase (Luc) reporter gene in the presence or absence of photoirradiation. Simultaneously, the cell viability was assessed by MTT assay (see Methods). Figure 3a shows the transfection efficiency and cytotoxicity of the pDNA/CP_4 polyplex and pDNA/CP_4/DPc ternary complexes with varying charge ratios of DPc after irradiation of the light with increasing fluence. In this experiment, the cells were photoirradiated after 6-h incubation with each complex and fresh medium replacement, followed by 48-h post-incubation. The 1:2:1 and 1:2:2 ternary complexes achieved more than 100-fold photochemical enhancement of the transgene expression with minimal photocytotoxicity over a wide range of fluence (-3.6 J cm^{-2}), whereas the 1:2:5 ternary complex, having a disordered structure, showed the lowest transfection activity (Fig. 3a). Note that a further increase in fluence resulted in a significant increase in the photocytotoxicity of the ternary complexes (a 50–70% decrease in the viability at 5.4 J cm^{-2}; see Supplementary Information, Fig. S1). The transfection to a different cell line (that is, 293T cells) revealed similar photochemical enhancement of transgene expression by the ternary complexes, although the 1:2:1 and 1:2:2 ternary complexes showed appreciable photocytotoxicity at a fluence higher than 2.7 J cm^{-2} (see Supplementary Information, Fig. S2A). Furthermore, when HeLa cells were incubated with the ternary complexes for a prolonged period (that is, 24 h) before photoirradiation, the results were similar to those in Fig. 3a (see Supplementary Information, Fig. S2B). The effect of PCI-mediated transfection was comparable to or more effective than that of hydroxychloroquine, a potent endosomotropic agent[21], depending on the cell lines (see Fig. 3a and Supplementary Information, Fig. S2A).

The effect of the ternary complex on the PCI-mediated transfection was further compared with that of $AlPcS_{2a}$ (aluminium phthalocyanine with two sulphonate groups on adjacent phthalate rings), which was demonstrated to be an effective photosensitizer in PCI[8–10]. Figure 3b shows the effect of $AlPcS_{2a}$ on the transfection efficiency of the pDNA/CP_4 polyplex (N/P ratio = 2) and cytotoxicity to HeLa cells with varying concentrations of $AlPcS_{2a}$ and fluence. In the system using $AlPcS_{2a}$, the photochemical enhancement of the transfection was accompanied by a significant increase in the photocytotoxicity, regardless of the concentrations of $AlPcS_{2a}$. Comparison between Fig. 3a and b reveals that the ternary complex achieved an expanded range of safe light doses,

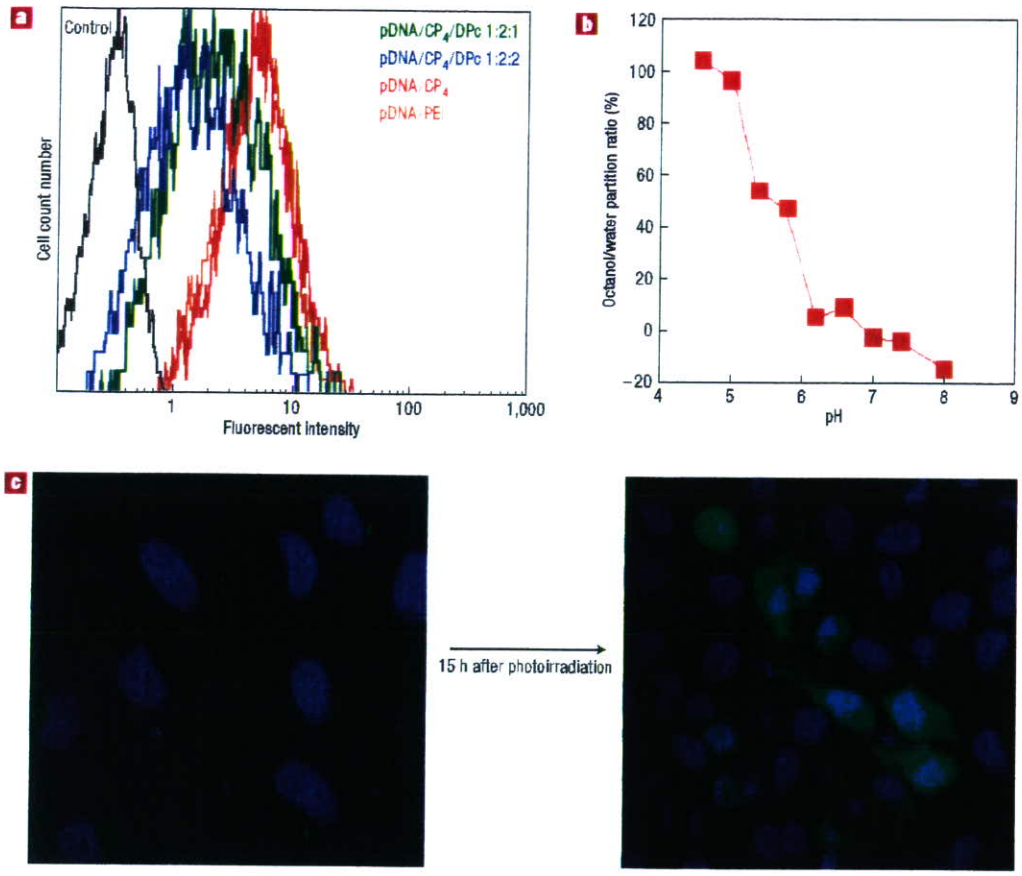

Figure 2 Properties of DPc and the pDNA/CP_4/DPc ternary complexes. a, Cellular uptake of the electrostatic complexes incorporating fluorescein-labelled pDNA. HeLa cells were incubated with each complex for 6 h, followed by flow cytometric analysis. The pDNA/PEI polyplex was prepared at an N/P ratio of 10. **b**, The pH-dependent partitioning (%) of DPc from the aqueous phase to the octanol phase. **c**, The intracellular distribution of FITC-dextran (green) co-incubated with the pDNA/CP_4/DPc complex with a charge ratio of 1:2:1 before and after photoirradiation. HeLa cells were incubated with the ternary complex for 6 h, followed by photoirradiation. The cell nuclei were stained with Hoechst 33258 (blue).

in which remarkable photochemical enhancement of the transgene expression was accomplished without compromising cell viability, ensuring the safety and effectiveness of the PCI-mediated *in vivo* gene delivery.

The reduced cytotoxicity after prolonged incubation with synthetic vectors might be one of the main criteria for successful *in vivo* transfection. In this study, the cells were photoirradiated after 6 h incubation with each complex, followed by 48-h post-incubation without medium replacement. Figure 3c shows the transfection efficiency and cytotoxicity of each complex after prolonged incubation. The 1:2:0.5, 1:2:1 and 1:2:2 ternary complexes showed 158-, 117- and 23-fold photochemical enhancement of the transfection, respectively, with approximately 20% decreases in the cell viability. In contrast, the efficient transfection by the PEI polyplex was accompanied by a remarkable decrease (~85%) in the cell viability. Thus, the PCI-mediated gene delivery can avoid long-term toxicity, which is often induced by the polyplexes based on buffering polycations, because the process toxic to the cell is controlled in a light-responsive manner. Also, the ternary complex with a negative ζ-potential value might hardly interact with the negatively charged cell membranes, leading to reduced cytotoxicity in long-term incubation.

The potential of the ternary complex for *in vivo* PCI-mediated gene delivery was studied by the transfection of a reporter gene (a variant of yellow fluorescent proteins, Venus) to the conjunctival tissue in rat eyes on laser irradiation. In this study, the rat eyes received a subconjunctival injection of the ternary complex (360° circumferential to the cornea), and part of the conjunctiva was then irradiated with a semiconductor laser (689 nm) at 2 h post-injection (Fig. 4a). The pDNA/CP_4/DPc ternary complex with a charge ratio of 1:2:1 achieved significant gene expression only at the laser-irradiated site in the conjunctiva in 8 out of 12 eyes (2 days after irradiation; Fig. 4b,c). Neither the ternary complexes with different compositions (that is, the 1:2:0.5 and 1:2:2 ternary complexes) nor ExGen500, which is one of the most efficient synthetic vectors, showed visible transgene expression. With the passage of time, the number of transfected eyes as well as the fluorescent intensity significantly decreased (Fig. 4c). Fluorescent microscopic observation of a frozen section of the conjunctival tissue revealed that the conjunctival epithelial cells were clearly transfected (Fig. 4d,e). Thus, the transfection only at the laser-irradiated site in the conjunctival tissue was achieved by the PCI-mediated gene delivery using the ternary complex. To our knowledge, this is the first success in PCI-mediated gene delivery *in vivo*.

PCI is a smart concept, which allows the cytoplasmic delivery of macromolecular compounds in a light-inducible

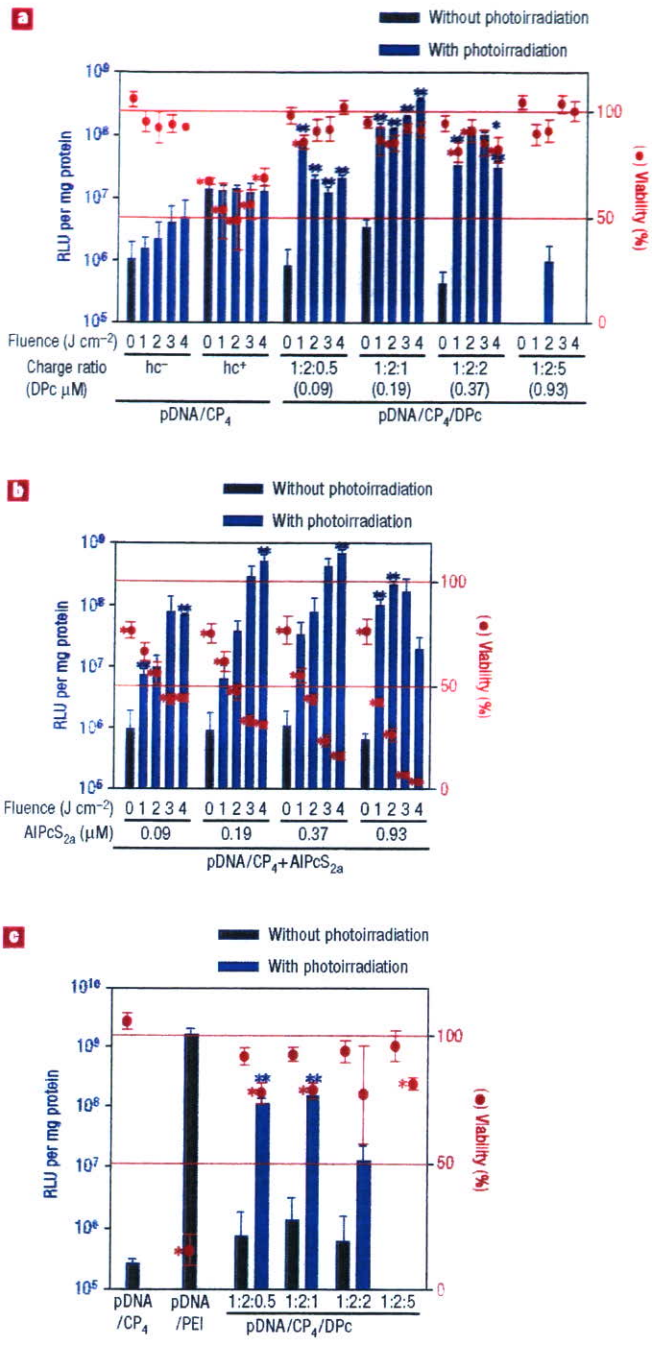

Figure 3 ***In vitro*** **tranfection efficiency and cytotoxicity to HeLa cells. a**, The effect of fluence on the transfection efficiency (bars) and photocytotoxicity (dots) of the pDNA/CP_4 and pDNA/CP_4/DPc complexes. Photoirradiation was performed 6 h after incubation with each complex, followed by 48 h post-incubation in a fresh medium. The hc represents hydroxychloroquine. **b**, The effect of fluence on the transfection efficiency (bars) and photocytotoxicity (dots) of the pDNA/CP_4 complex with different concentrations of $AlPcS_{2a}$. The same experimental conditions as **a** were applied. **c**, The transfection efficiency (bars) and photocytotoxicity (dots) when HeLa cells were irradiated 6 h after incubation with each complex at 3.6 J cm^{-2}, followed by 48 h post-incubation without medium replacement. Results are expressed as mean ± s.d. ($n = 4$). The unpaired t-test was used for statistical analysis, and significant changes in the cell viability (treated to untreated) and the transfection efficiency (photoirradiated to non-photoirradiated) are indicated by asterisks * and **, respectively.

manner. In previous studies, it was demonstrated that $AlPcS_{2a}$ and $TPPS_{2a}$ (meso-tetraphenylporphine with two sulphonate groups on adjacent phenyl rings) were effective in PCI-mediated delivery[8–10]. It is assumed that a hydrophobic moiety in these dissymmetric compounds may provide preferable interaction with cell membranes, whereas they are internalized by endocytosis because of high water solubility. However, such an amphiphilic nature of the compounds should generate interaction with the plasma membrane to some extent, possibly photodamaging the plasma membrane. Meanwhile, such amphiphilic photosensitizers may relocalize to some cytoplasmic organelles such as mitochondria and endoplasmic reticulum during the photoirradiation[11,22,23]. It is known that the plasma membrane and some cytoplasmic organelles might be susceptible to the photocytotoxicity[11]. These effects may be a major cause of the photocytotoxicity of $AlPcS_{2a}$ and $TPPS_{2a}$. These compounds are still useful in PCI; however, reduced photocytotoxicity might be desired before considering further applications of this technology. We assume that the selective photodamage of the endosomal membrane is a key to reduced photocytotoxicity in PCI, motivating us to develop different gene carriers based on the PCI concept.

To design gene carriers based on the PCI concept, the following points should be considered. (i) For *in vivo* applications, the photosensitizing units should be integrated into gene carriers as one component, because separate administration of photosensitizers might result in their diffused localization to the surrounding tissues, which may decrease the efficiency in the PCI-mediated gene delivery and cause the phototoxicity to the surrounding tissues. (ii) Following internalization by the endocytosis, the photosensitizers should be released from gene carriers, otherwise, pDNA could be photochemically inactivated on photoirradiation. (iii) The photosensitizers should have increased affinity for cell membranes under endosomal conditions to accomplish the photochemical rupture of the endosomal membrane. In the ternary complex system, we suggest that DPc may be released from the complex to interact with the endosomal membrane (Fig. 2b), satisfying the aforementioned requirements for effective PCI-mediated gene delivery (Fig. 5).

In *in vitro* experiments, both the ternary complex and the PCI using $AlPcS_{2a}$ showed reduced cell viability as the fluence increased, and the degree of the cytotoxicity depended on the cell lines (Fig. 3a,b, and see Supplementary Information, Figs S1 and S2). Indeed, the PCI conditions have been optimized depending on each cell line[9,10]. However, in this study, a comparison under the same experimental conditions revealed that the ternary complex showed a wider range of safe light doses, in which remarkable enhancement of the transfection was accomplished without reduced cell viability, irrespective of cell lines and incubation time (Fig. 3a and see Supplementary Information, Fig. S2). These results may be due to control of the initial steps in the PCI and highly selective photodamage to the endosomal membrane as described above. We believe that such an expanded range of safe light dose might have resulted in our success in the PCI-mediated gene delivery *in vivo*.

The reduced photocytotoxicity of the ternary complexes might be one of the most important achievements in this study. Because of the pH-dependent membrane binding ability of DPc (Fig. 2b), the photocytotoxicity seems to be reduced when DPc is relocated from the acidic endocytic vesicles into the cytosol. A cytosolic localization of DPc may not be expected to cause phototoxicity owing to low stability of singlet oxygen in aqueous media. Alternatively, it seems that DPc may undergo slower diffusion in the cytosol because of its larger size compared with $AlPcS_{2a}$ and have a reduced chance of relocalizing in susceptible cytoplasmic organelles. However, these assumptions remain to be clarified.

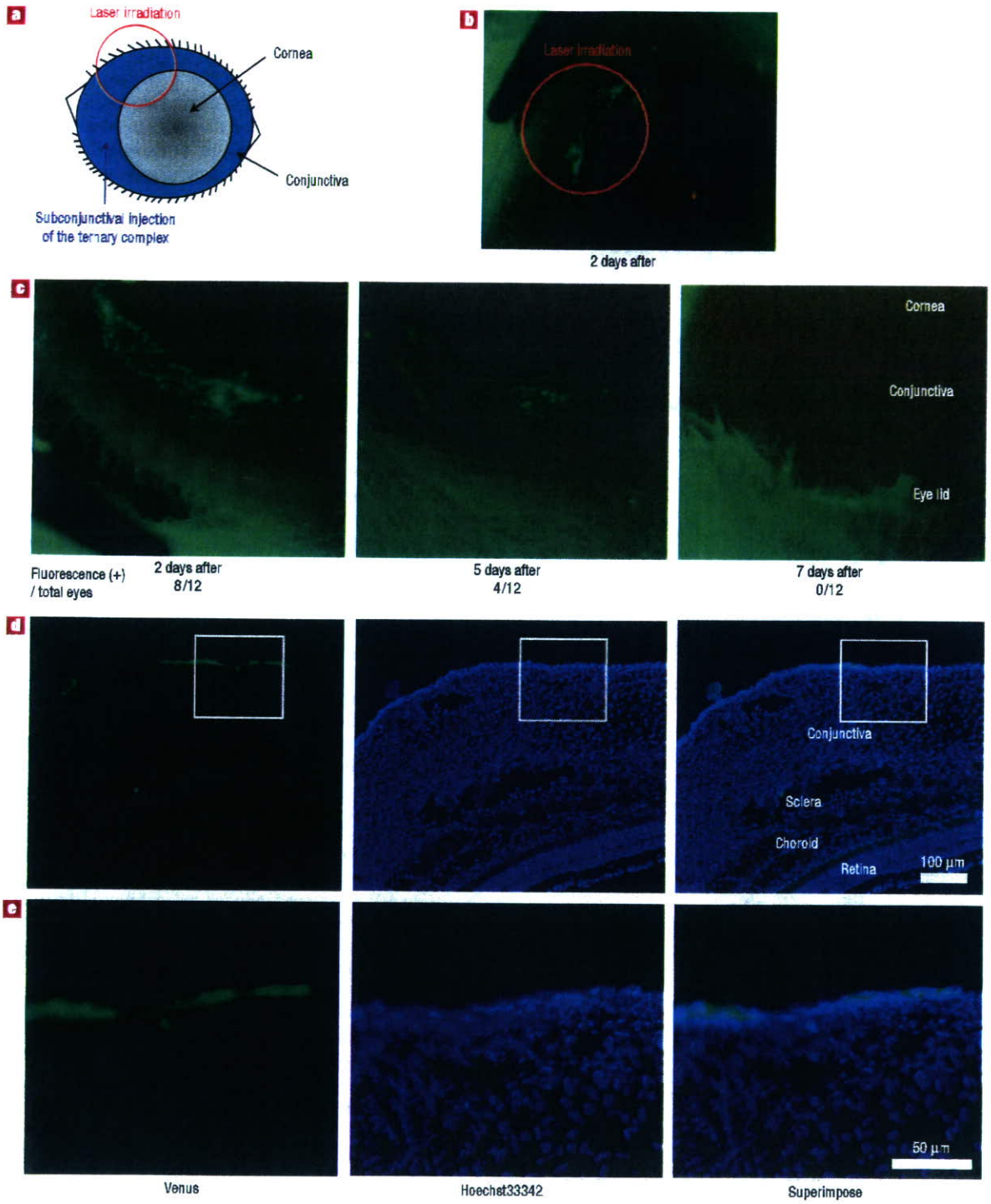

Figure 4 Transfection to the conjunctival tissue to rat eyes. a, The scheme for *in vivo* transfection. Rats were given a subconjunctival injection (coloured in light blue) of each complex containing 15 μg pDNA encoding a variant of a yellow fluorescent protein (Venus). At 2 h post-injection, a part of the conjunctiva (red circle) was irradiated with a light of 689 nm. **b**,**c**, Fluorescent images of the Venus expression in the rat eye at 2, 5 and 7 days after the photochemical transfection using the 1:2:1 ternary complex. The fluorescent-positive eyes/total eyes are indicated below the images. **d**, A fluorescent image of the Venus expression in the frozen section of the conjunctival tissue. The image was taken 2 days after the photochemical transfection using the pDNA/CP_4/DPc 1:2:1 ternary complex. The cell nuclei were stained in blue. **e**, A magnified image of the white square in the above fluorescent image.

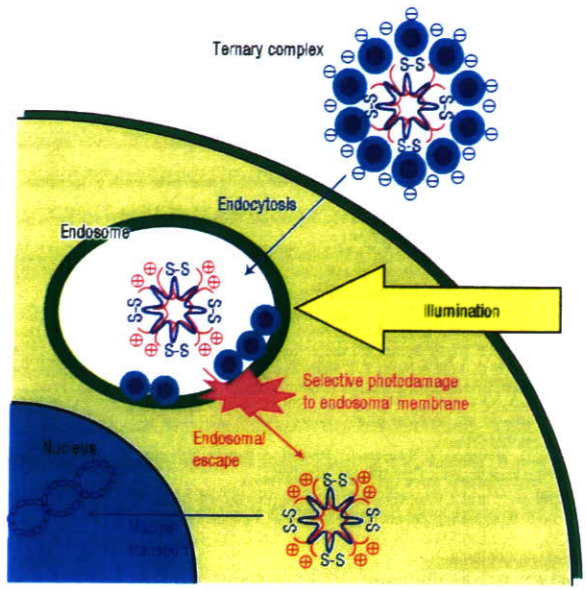

Figure 5 A scheme for itinerary of the ternary complex to the transgene expression. The ternary complex was designed to control the initial steps (that is, internalization by the endocytosis and photodamage of the endosomal membrane to release the polyplex to the cytoplasm) in the PCI-mediated gene delivery.

In the ternary complex system, there is still room for optimization of each component. For example, the polyplex-forming polycations can be optimized, because a variety of polycations can be used for the formation of the ternary complex. Indeed, the ternary complex was formed from poly(L-lysine) at a charge ratio of 1:2:2 (see Supplementary Information, Table S1), and the pDNA/poly(L-lysine)/DPc ternary complex showed approximately 15-fold photochemical enhancement of the transfection with a 50% decrease in the cell viability (see Supplementary Information, Fig. S3). This result suggests that the polyplex-forming polycations significantly affect the transfection efficiency and cytotoxicity, highlighting the importance of optimization of the polycations. In the present study, the CP_4 peptide, of which the nuclear localization and the effective gene transfection following the translocation into the cytoplasm were demonstrated in the previous study[17], was used to prepare the ternary complex, and we successfully obtained the PCI-mediated gene transfection *in vitro* and *in vivo*. Further optimization of the polycations is our future interest, and the studies in this direction will be reported elsewhere.

This system can be potentially useful for the gene therapy of ophthalmic diseases[24]. The molecular design could be expanded to a systemically targeted gene carrier for the treatment of various diseases, including solid tumours. Spatial control of transgene expression in the body will ensure the effectiveness and safety of *in vivo* gene therapy.

METHODS

POLYMER SYNTHESIS AND CHARACTERIZATION

Synthesis of ionic DPc (Fig. 1a) was performed according to the method reported in ref. 25. The detailed synthetic procedure is described in Supplementary Information. The absorption spectra revealed that DPc shows B band absorption at 350 nm and strong Q band absorption at 685 nm.
A cationic peptide C(YGRKKRRQRRRG)$_2$ (CP_2) was synthesized by the Peptide Institute (Osaka, Japan). The CP_4 peptide was prepared by oxidation of the CP_2 peptide in 10 mM of Tris–HCl buffer (pH 7.4) over 14 days. PAA homopolymer (DP: 26; weight-averaged/number-averaged molecular mass (M_w/M_n), 1.2) was synthesized as reported in ref. 26.

PLASMID DNA

A plasmid DNA, pCAcc+Luc, containing a firefly luciferase cDNA driven by a CAG promoter[27] was provided by RIKEN Bioresource Centre (Tsukuba, Japan). Also, a fragment cDNA of SEYFP-F46L (Venus), which is a variant of a yellow fluorescent protein with the mutation F46L[28], was provided by A. Miyawaki of the Brain Science Institute, RIKEN (Wako, Japan), and inserted into the pCAcc vector (pCAcc+Venus). Each plasmid DNA (pDNA) was amplified in competent DH5α *Escherichia coli* and purified by a HiSpeed Plasmid Maxi Kit (Qiagen, Germany). pCAcc+Luc was used for *in vitro* studies, whereas *in vivo* transfection was performed using pCAcc+Venus.

PREPARATION OF THE TERNARY COMPLEX

The pDNA/CP_4 polyplex was prepared by mixing pDNA and CP_4 peptide in 10 mM of Tris–HCl buffer (pH 7.4) at an N/P ratio of 2 (pDNA concentration, 100 μg ml^{-1}). At 30 min after incubation at ambient temperature, the pDNA/CP_4 polyplex solution was mixed with the DPc solution with varying charge molar ratios of pDNA/CP_4/DPc, followed by an extra 30-min incubation at ambient temperature to obtain the pDNA/CP_4/DPc ternary complex. The ternary complexes with varying ratios of DPc were characterized by a gel retardation assay.

CHARACTERIZATION OF THE TERNARY COMPLEX

The size and polydispersity were evaluated by dynamic light scattering measurements using a DLS-7000 instrument (Otsuka Electronics, Osaka, Japan) equipped with an Ar-ion laser (488 nm). The ζ-potential was measured by a laser-Doppler electrophoresis ELS-6000 instrument (Otsuka Electronics) equipped with a He–Ne ion laser (633 nm). AFM imaging was performed in a tapping mode with a standard silicon probe 160 μm in length using an NVB 100 microscope (Olympus, Tokyo, Japan) operated by Nanoscope IIIa software (Digital Instruments, Santa Barbara, California). Detailed experimental conditions are described in the Supplementary Information.

OCTANOL/WATER PARTITIONING

The experimental procedure is described in the Supplementary Information.

FLOW CYTOMETRY ANALYSIS AND CONFOCAL MICROSCOPIC OBSERVATION

The amount of uptake of each polyplex containing pDNA labelled with fluorescein by HeLa cells was analysed by flow cytometry. The detailed experimental conditions are described in the Supplementary Information. Confocal observation of FITC-labelled dextran (M_w: 10,000–15,000) co-incubated with the 1:2:1 ternary complex in HeLa cells before and after photoirradiation was performed using LSM510 (Carl Zeiss, Jena, Germany). Detailed experimental conditions are provided in the Supplementary Information.

IN VITRO TRANSFECTION STUDY

HeLa cells (10,000 cells) on a 24-well culture plate were incubated with each polyplex containing 1 μg pDNA in 0.5 ml of Dulbecco's Modified Eagle's Medium (DMEM) containing 10% fetal bovine serum (FBS), followed by 6- or 24-h incubation and fresh medium replacement. The culture plates were photoirradiated using a 300-W halogen lamp (fluence rate, 3.0 mW cm^{-2}) equipped with a band-pass filter (400–700 nm) with increased fluence (0.9–3.6 J cm^{-2}). After 48 h post-incubation, the transfection efficiency was evaluated by the Luciferase Assay System (Promega, Madison, Wisconsin) and a Lumat LB9507 luminometer (Berthold Technologies, Bad Wildbad, Germany), whereas the cell viability was evaluated by the 3-(4,5-dimethylthiazol-2-yl)-2,5-diphenyltetrazolium bromide (MTT) assay. Sulphonated aluminium phthalocyanine ($AlPcS_{2a}$) and PEI (25 kDa) were purchased from Frontier Scientific (Logan, Utah) and Sigma-Aldrich (St Louis, Missouri), respectively.

IN VIVO TRANSFECTION TO CONJUNCTIVA

Wistar rats (male, 6 weeks old, number of animals $n = 12$; Saitama Experimental Animal Supply, Saitama, Japan) were given a subconjunctival injection of 150 μl of each complex containing 15 μg pDNA (pCAcc+Venus). At 2 h post-injection, the rats were anesthetized and part of the conjunctiva was irradiated using a 689-nm semiconductor laser emitted from laser equipment built in-house (Topcon, Tokyo, Japan) with 2.0 mW laser power and 4 mm projection diameter for 60 s (1 J cm^{-2}). The fluorescent images of the Venus

expression in a rat eye and the conjunctival tissues were taken as described in Supplementary Information. All the experimental procedures were handled in accordance with the guidelines of the Animal Committee of the University of Tokyo. The polyplex from linear PEI, with ExGen500 (Fermentas, Vilnius, Lithuania) as a control vector, was prepared at N/P ratio = 6.

Received 12 July 2005; accepted 28 September 2005; published 20 November 2005.

References

1. Ogris, M. & Wagner, E. Targeting tumors with non-viral gene delivery systems. *Drug Discov. Today* **7**, 479–485 (2002).
2. Taira, K., Kataoka, K. & Niidome, T. (eds) *Non-viral Gene Therapy: Gene Design and Delivery* (Springer, Tokyo, 2005).
3. Merdan, T., Kopecek, J. & Kissel, T. Prospects for cationic polymers in gene and oligonucleotide therapy against cancer. *Adv. Drug Deliv. Rev.* **54**, 715–758 (2002).
4. Salem, A. K., Searson, P. C. & Leong, K. W. Multifunctional nanorods for gene delivery. *Nature Mater.* **2**, 668–671 (2003).
5. Behr, J. P. The proton sponge. A trick to enter cells the viruses did not exploit. *Chimia* **51**, 34–36 (1997).
6. Berg, K. *et al.* Photochemical internalization: a novel technology for delivery of macromolecules into cytosol. *Cancer Res.* **59**, 1180–1183 (1999).
7. Høgset, A., Prasmickaite, L., Tjelle, T. E. & Berg, K. Photochemical transfection: A new technology for light-induced, site-directed gene delivery. *Hum. Gene Ther.* **11**, 869–880 (2000).
8. Prasmickaite, L., Høgset, A. & Berg, K. Evaluation of different photosensitizers for use in photochemical gene transfection. *Photochem. Photobiol.* **73**, 388–395 (2001).
9. Høgset, A. *et al.* Photochemical transfection: A technology for efficient light-directed gene delivery. *Somat. Cell Mol. Genet.* **27**, 97–113 (2002).
10. Høgset, A. *et al.* Photochemical internalization in drug and gene delivery. *Adv. Drug Deliv. Rev.* **56**, 95–115 (2004).
11. Macdonald, I. J. & Dougherty, T. J. Basic principle of photodynamic therapy. *J. Porphyrins Phthalocyanines* **5**, 105–129 (2001).
12. Esfand, R. & Tomalia, D. A. Poly(amidoamine) (PAMAM) dendrimers: from biomimicry to drug delivery and biomedical applications. *Drug Discov. Today* **6**, 427–436 (2001).
13. Gillies, E. R. & Frechet, J. M. Dendrimers and dendritic polymers in drug delivery. *Drug Discov. Today* **10**, 35–43 (2005).
14. Duncan, R. The dawning era of polymer therapeutics. *Nature Rev. Drug Discov.* **2**, 347–360 (2003).
15. Kobayashi, H. *et al.* Lymphatic drainage imaging of breast cancer in mice by micro-magnetic resonance lymphangiography using a nano-size paramagnetic contrast agent. *J. Natl Cancer Inst.* **96**, 703–708 (2004).
16. Tang, M., Redemann, C. T. & Szoka, F. C. Jr. In vitro gene delivery by degraded polyamidoamine dendrimers. *Bioconjugate Chem.* **7**, 703–714 (1996).
17. Rudolph, C. *et al.* Oligomers of the arginine-rich motif of the HIV-1 TAT protein are capable of transferring plasmid DNA into cells. *J. Biol. Chem.* **278**, 11411–11418 (2003).
18. Caruso, F., Caruso, R. A. & Möhwald, H. Nanoengineering of inorganic and hybrid hollow spheres by colloidal templating. *Science* **282**, 1111–1114 (1998).
19. Donath, E. *et al.* Novel hollow polymer shells by colliid-templated assembly of polyelectrolytes. *Angew. Chem. Int. Edn* **37**, 2002–2005 (1998).
20. Levitan, H. & Barker, J. L. Salicylate. Structure-activity study of its effects on membrane permeability. *Science* **176**, 1423–1425 (1972).
21. Itaka, K. *et al.* in *Carrier-Based Drug Delivery* (ed. Svenson, S.) 154–159 (ACS Symp. Series Vol. 879, Americal Chemical Society, 2004).
22. Moan, J., Berg, K., Anholt, A. & Madslien, K. Sulfonated aluminum phthalocyanines as sensitizers for photochemotherapy. Effects of small doses on localization, dye fluorescence and photosensitivity in V79 cells. *Int. J. Cancer* **58**, 865–870 (1994).
23. Rodal, G. H., Rodal, S. K., Moan, J. & Berg, K. Liposome-bound Zn(II)-phthalocyanine. Mechanisms for cellular uptake and photosensitization. *J. Photochem. Photobiol. B* **45**, 150–159 (1998).
24. Daiger, S. P. Was the human genome project worth the efforts? *Science* **308**, 362–364 (2005).
25. Ng, A. C. H., Li, X. & Ng, D. K. P. Synthesis and photophysical properties of nonaggregated phthalocyanines bearing dendritic substitutes. *Macromolecules* **32**, 5292–5298 (1999).
26. Harada, A. & Kataoka, K. Formation of polyion complex micelles in aqueous milieu from a pair of oppositely-charged block copolymers with poly(ethylene glycol) segments. *Macromolecules* **28**, 5294–5299 (1995).
27. Niwa, H., Yamamura, K. & Miyazaki, J. Efficient selection for high-expression transfectants with a novel eukaryotic vector. *Gene* **108**, 193–199 (1991).
28. Nagai, T. *et al.* A variant of yellow fluorescent protein with fast and efficient mutation for cell-biological applications. *Nature Biotechnol.* **20**, 87–90 (2002).

Acknowledgements

We thank N. Kanayama (the University of Tokyo), S. Kawauchi (National Defense Medical College) and K. Date (the University of Tokyo) for technical assistance. This work was supported in part by the Core Research Program for Evolutional Science and Technology (CREST) from Japan Science and Technology Agency (JST).

Correspondence and requests for materials should be addressed to K.K.[3]

Supplementary Information accompanies this paper on www.nature.com/naturematerials.

Competing financial interests

The authors declare that they have no competing financial interests.

Cell Transplantation, Vol. 14, pp. 695–700, 2005
Printed in the USA.

0963-6897/05 $20.00 + .00
E-ISSN 1555-3892
www.cognizantcommunication.com

Time Course Evaluation of Reparative Cartilage With MR Imaging After Autologous Chondrocyte Implantation

Atsuya Watanabe,*† Yuichi Wada,* Takayuki Obata,† Takahisa Sasho,* Takuya Ueda,‡ Mitsuru Tamura,† Hiroo Ikehira,† and Hideshige Moriya*

*Department of Orthopaedic Surgery, Graduate School of Medicine, Chiba University, Chiba, 260-8677 Japan
†National Institute of Radiological Sciences, Chiba, 263-8555 Japan
‡Department of Radiology, Graduate School of Medicine, Chiba University, Chiba, 260-8677 Japan

The aim of this study was to evaluate the qualitative change in reparative cartilage after autologous chondrocyte implantation (ACI). Ten knees of 10 patients were studied. The signal intensities of reparative and normal cartilage were evaluated by fat-suppressed three-dimensional spoiled-gradient recalled (FS 3D-SPGR) MR imaging. The signal intensity (SI) index (signal intensity of reparative cartilage divided by that of normal cartilage) was defined and the change in SI index was investigated. Histological and biochemical evaluation was done at the second look arthroscopy. The SI index was at its lowest level immediately after ACI and increased with time to 9 months thereafter. After 9–12 months, the SI index settled to almost level and was maintained at that value for at least 2–3 years postoperatively. The average of the SI indexes after 12 months to the last examination was 74.2 ± 4.6 (range 64.2–82.8), which means signal intensity of reparative cartilage was maintained at a value lower than that of normal cartilage. The total ICRS score was 11.6 ± 2.3 points (mean ± SD). The GAG concentration was 107.9 ± 17.0 μg/mg (mean ± SD) in normal cartilage and 65.9 ± 9.4 μg/mg in reparative cartilage. The quality of reparative cartilage as hyaline cartilage was inferior to that of normal cartilage. In the present study, the time course change in the SI index indicates that the major maturation process of implanted chondrocytes neared completion in 9–12 months. Minor changes, such as matrix remodeling with reorganization of the collagen fibers in reparative cartilage, may continue, but an almost identical condition seemed to be maintained during the first 2–3 years of follow-up. SI index does not always reflect all properties of reparative cartilage but may be a useful parameter for noninvasive evaluation.

Key words: Autologous chondrocyte implantation; Magnetic resonance imaging; Time course evaluation; Signal intensity; Reparative cartilage

INTRODUCTION

Autologous chondrocyte implantation (ACI) has recently become a widely used technique for articular cartilage lesions. Formerly, it was known as an effective, essential treatment, especially for the large osteochondral defects of knee articular cartilage (15).

Until now, most follow-up studies of ACI treatment in humans have been conducted by using clinical assessments; however, only a few follow-up studies concerning the qualitative aspect of reparative cartilage have been conducted (15). One of the reasons for the small number of follow-up studies has been that the qualitative evaluation of reparative cartilage could be achieved only by invasive methods, such as arthroscopy with biopsy.

The aim of this study was to evaluate the time course change of quality in reparative cartilage after ACI by using magnetic resonance (MR) imaging. We performed fat-suppressed three-dimensional spoiled-gradient recalled (FS 3D-SPGR) MR imaging to investigate the changes of signal intensity in reparative cartilage. With this imaging technique, normal articular cartilage appears higher in signal intensity than adjacent structures (6). Histological and biochemical evaluation of reparative cartilage was done at the second-look arthroscopy to assess how closely the reparative cartilage resembled normal cartilage.

MATERIALS AND METHODS

The knees of 10 patients (seven males and three females) were investigated after the patients had undergone ACI of the femoral condyle (seven medial femoral

Address correspondence to Atsuya Watanabe, Department of Orthopaedic Surgery, Graduate School of Medicine, Chiba University, 1-8-1, Inohana, Chuo-Ku, Chiba-Shi, 260-8677 Japan. Tel: 81-43-226-2117; Fax: 81-43-226-2116; E-mail: atsuyan1@pa2.so-net.ne.jp

condyles and three lateral femoral condyles). The patients' mean age at the time of ACI was 21.2 ± 7.5 years (range 13–35 years), and the mean size of the defect was 4.5 ± 2.1 cm^2 (range 2.3–10.5 cm^2). This study was approved by the ethics review committee of Chiba University Hospital, and informed consent was obtained from all patients.

ACI was performed according to the method described by Brittberg and colleagues (3). In brief, healthy cartilage was obtained from a non-weight-bearing area of the affected knee during an initial arthroscopy. Chondrocytes were then isolated from the cartilage and cultured in the laboratory for about 4 weeks (Genzyme Tissue Repair, Cambridge, MA). The cultured chondrocytes were injected into the defect, which was covered by a periosteal flap that had been removed from the tibia. The rehabilitation schedule included active movement of the knee, which was started immediately after surgery. Weight bearing was gradually introduced at 6 weeks after ACI and increased to full weight bearing by 10 weeks after ACI.

FS 3D-SPGR MR imaging was performed in the sagittal plane at 0, 3, 6, 9, 12, 18, 24, and 36 months after ACI using an MR imaging system at 1.5 Tesla with a dedicated knee coil (Signa Horizon General Electronic, Milwaukee, WI) (In three cases, imaging was performed up to 24 months.) The scanning parameters were 52 ms repetition time, 10 ms echo time, 60° flip angle, 130 × 130 mm field of view, 1.5 mm section thickness, and 512 × 512 matrix. To compare the signal intensity of reparative cartilage with that of normal cartilage over time, we defined the signal intensity (SI) index (signal intensity of reparative cartilage divided by the signal intensity of normal cartilage) and expressed it as a percentage. We investigated the change in SI index during the observation period.

It is known that the signal intensity on MR images by FS 3D-SPGR imaging is given by the equation:

$$SI = \{k \cdot \rho[1 - \exp(-TR/T_1)]\sin\alpha\}/[1 - \cos\alpha \cdot \exp(-TR/T_1)]$$

where k is the constant factor determined by the imaging apparatus, ρ is proton density, α is flip angle, TR is repetition time, and T_1 is longitudinal relaxation time.

The T_1 of articular cartilage may vary depending on the histological and biochemical characteristics of the cartilage. With this imaging technique, a strong T_1 weighted image is obtained and signal intensity is considered to mainly reflect the tissue-specific T_1 when the imaging apparatus and scanning parameters are the same. To verify that the signal intensity of reparative cartilage and normal cartilage in FS 3D-SPGR MR images represented the T_1 of the two cartilages, T_1 measurements were performed.

T_1 measurements were performed at 21.2 ± 10.4 months (range 13–38 months) after ACI by using a MR imaging system at 1.5 Tesla (Gyroscan Intera; Philips Medical Systems, Holland). A time course T_1 measurement was also performed for a patient at 1, 4, 8, 12, 18, and 24 months after ACI. Inversion recovery turbo-spin echo images were obtained at six inversion times: 50, 100, 200, 400, 800, and 1600 ms. The scanning parameters were 1800 ms repetition time, 28 ms echo time, 130 × 130 mm field of view, 3.0 mm section thickness, 512 × 512 matrix, and 6 turbo spin echo factor. T_1 calculated maps were generated from inversion recovery images, using the commercially available software, Dr. View (Asahikasei; Tokyo, Japan), and the T_1s of reparative cartilage and normal cartilage were investigated. We investigated the change of T_1 in the patient who underwent time course T_1 measurement.

For the signal intensity and T_1 measurements, the region of interest (ROI) was drawn in the whole area of reparative cartilage. The hypertrophic periosteum (if it existed) was not included in the ROI. The ROI of normal cartilage was drawn in the weight-bearing area of the femoral condyle about 2 cm apart from the reparative cartilage (to avoid including the damaged cartilage near reparative cartilage). To standardize the procedure, all ROIs were drawn by the same investigator.

A second-look arthroscopy with biopsy was performed at 12.3 ± 0.5 months (range 12–13 months) after ACI surgery. Using an 11-gauge biopsy needle (Trapsystem MDTECH, Gainesville, FL), we took biopsies from all cases of reparative cartilage and from seven cases of normal cartilage. Reparative cartilage was stained with hematoxylin and eosin (H&E) and toluidine blue (TB) for general histology and the assessment of metachromasia. The International Cartilage Repair Society (ICRS) assessment form for repair of cartilage (14) was used to score the histological appearance of reparative cartilage (Table 1). The concentration of glycosaminoglycan (GAG), a major macromolecular constituent of articular cartilage, that was obtained from biopsy was evaluated with high-performance liquid chromatography in nine cases of reparative cartilage and seven cases of normal cartilage.

The Lysholm score (13) was performed to quantify the clinical status of the patients before ACI, 1 year after ACI, and at the time of the last evaluation (30.6 ± 8.9 months, range 18–47 months, after the ACI).

A t-test was used for statistical evaluation and significant difference was defined as $p < 0.05$.

RESULTS

In the MR images of a typical case, the signal intensity of reparative cartilage appeared low immediately after ACI, but it increased and approached that of normal cartilage with time (Fig. 1).

In all cases, the SI index fell to its lowest level imme-

Table 1. ICRS Visual Histological Assessment Scale

Feature	Score
1. Surface	
Smooth/continuous	3
Discontinuities/irregularities	0
2. Matrix	
Hyaline	3
Mixture: hyaline/fibrocartilage	2
Fibrocartilage	1
Fibrous tissue	0
3. Cell distribution	
Columnar	3
Mixed/columnar-clusters	2
Clusters	1
Individual cells/disorganized	0
4. Cell population viability	
Predominantly viable	3
Partially viable	2
<10% viable	0
5. Subchondral bone	
Normal	3
Increased remodeling	2
Bone necrosis/granulation tissue	1
Detached/fracture/callus at base	0
6. Cartilage mineralization (calcified cartilage)	
Normal	3
Abnormal/inappropriate location	0

diately after ACI but increased rapidly for 9 months thereafter. After 9–12 months, the SI index settled to almost level and was maintained at that value for at least 2–3 years postoperatively (Fig. 2). The average of the SI indexes from 12 months to the last examination was 74.2 ± 4.6 (range 64.2–82.8). This average means that the signal intensity of reparative cartilage was maintained at a value lower than that of normal cartilage.

The T_1 of reparative cartilage was significantly higher than that of normal cartilage, 1.34 ± 0.13 and 1.03 ± 0.08 s, respectively ($p < 0.05$). The T_1 in the patient who underwent time course T_1 measurement was at its highest level immediately after ACI, decreased with time to 9 months, and settled to almost level after that, which was compatible with the change of SI index (Fig. 3).

The average ICRS score of each criteria (see Table 1) was: 1) 1.2 ± 1.5 points, 2) 2.5 ± 0.7 points, 3) 1.6 ± 0.5 points, 4) 1.4 ± 0.8 points, 5) 1.9 ± 0.3 points, 6) 3.0 ± 0 points; the total was 11.6 ± 2.3 points. The histological appearance of reparative cartilage after ACI was not as good as that of normal cartilage.

The GAG concentration obtained from biopsy was 107.9 ± 17.0 μg/mg in normal cartilage and 65.9 ± 9.4 μg/mg in reparative cartilage. This difference in concentration was statistically significant ($p < 0.05$). In fact, the GAG concentrations of reparative cartilage were lower than normal cartilage in all cases.

There was a significant improvement in patients' Lysholm scores from a mean of 63.0 ± 12.2 points before surgery to 94.9 ± 5.1 points 1 year after surgery, and 97.7 ± 4.9 points at the time of the last evaluation.

DISCUSSION

The T_1 in cartilage may be shortened by decreased water content, increased concentration of macromolecular matrix components, and increased regularity of the collagen network structure (9). The time course change in the SI index that we observed may have been caused by changes in T_1 during the maturing process of the transplanted chondrocytes from the state of suspension to hard hyaline-like cartilage. Indeed, the T_1 in reparative cartilage decreased with time after grafting in this

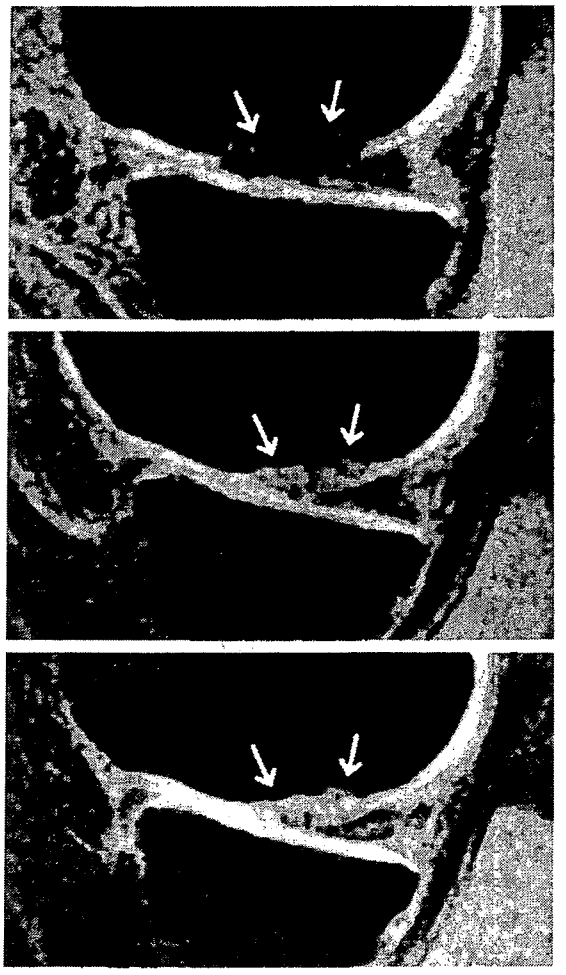

Figure 1. The time course change of signal intensity in three-dimensional spoiled gradient-recalled (3D-SPGR) magnetic resonance (MR) images of a typical case. The signal intensity of reparative cartilage (arrows) appeared low immediately after autologous chondrocytes implantation (ACI), but it increased and approached that of normal cartilage with time. (a) MR image immediately after ACI, (b) MR image 3 months after ACI, (c) MR image 12 months after ACI.

study. In simple words, as the reparative cartilage became more compatible with normal hyaline cartilage, the SI index increased. The SI index does not always reflect all properties of reparative cartilage but may be a useful parameter of changes in reparative cartilage in noninvasive evaluation.

Several animal studies on ACI concerning time course change of reparative cartilage have been done. However, differences in the outcomes between animals studied have been shown. For example, in a rabbit study, the reparative tissue appeared to mature towards hyaline cartilage for about 3 months, and an almost identical condition was maintained after that (4). In contrast, in a canine study, the reparative tissue appeared to mature for about 3–6 months, but the reparative cartilage appeared to become progressively damaged after that (1). Why there should be this apparent difference between animal species is unclear. In humans, the literature contains only a few reports that focus on the time course of cartilage maturation. The main maturation process of implanted cartilage in humans is believed to near completion within 1 year after implantation (10,11,17). In the present study, the time course change in the SI index that we observed indicates that the major maturation process of implanted chondrocytes neared completion in 9–12 months. We also observed that the quality of reparative cartilage as hyaline cartilage was inferior to that of normal cartilage. Minor changes, such as matrix remodeling with reorganization of the collagen fibers in reparative cartilage, may continue, but an almost identical condition was maintained during the first 2–3 years of follow-up. This is similar to the impression obtained from clinical results that it reached nearly full marks 1 year after operation and was maintained until the time of the final observation.

Evaluation of the maturation process of reparative cartilage is important in determining postoperative treatment such as adjustment of weight bearing and restrictions of activity. Evaluation of reparative cartilage after maturation is also important in assessing treatment results and predicting outcomes such as the presence or absence of long-term degenerative changes. This study suggested that the first 9 months after ACI were important because the histological success of reparative cartilage might be determined. Adjustments of the postoperative treatment, which could influence maturation of the reparative tissue, during this period could result in making reparative cartilage that is closer to normal hyaline cartilage.

Histology of reparative cartilage after ACI has been

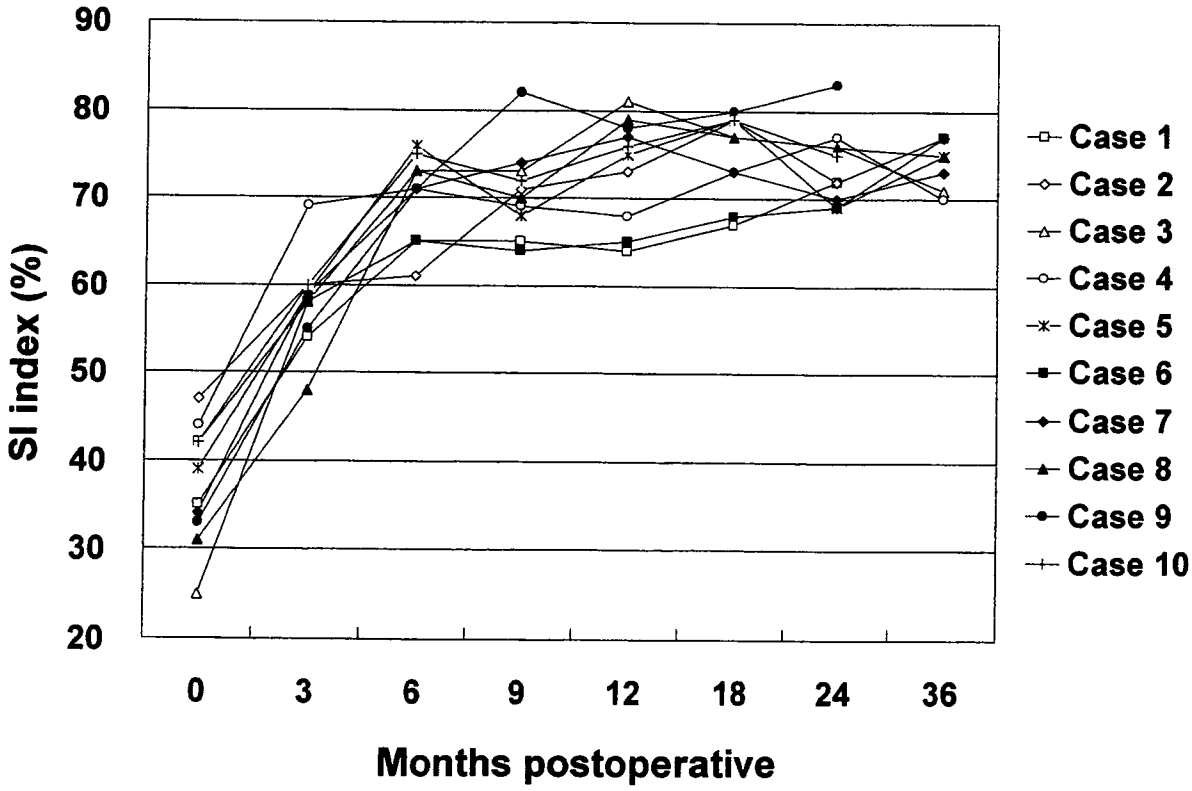

Figure 2. The signal intensity (SI) index after autologus chondrocytes implantation. The SI index was at its lowest level immediately after ACI and increased with time to 9 months thereafter. After 9–12 months, the SI index settled to almost level and was maintained at that value for at least 2–3 years postoperatively.